Computers and Geotechnics xxx (xxxx) xxx–xxx

Contents lists available at ScienceDirect

Computers and Geotechnics

journal homepage: www.elsevier.com/locate/compgeo

Research Paper

On the computational applicability of the modified Cam-clay model on the 'dry' side

Apostolos Vrakas

Institute for Geotechnical Engineering, ETH Zurich, Stefano-Franscini-Platz 5, 8093 Zurich, Switzerland

ARTICLE INFO

Keywords:
Cam-clay plasticity
Local uniqueness
Overconsolidation
Snap-back
Softening

ABSTRACT

This paper presents a theoretical investigation into the behaviour of the modified Cam-clay model on the 'dry' side and shows that: (a) for arbitrary strain-controlled loadings, local uniqueness is violated when the stress ratio η exceeds a certain critical value η_d; (b) for triaxial loadings, local uniqueness is violated when η exceeds another critical value, lower or equal to η_d, and the predicted response to a strain-controlled process becomes plastically inadmissible, while the response to a stress-controlled process presents a 'snap-back'; (c) stress-point algorithms and displacement-based numerical analysis codes can provide nonsensical results in such cases, which violate plasticity theory.

1. Introduction

The necessary conditions that an elasto-plastic constitutive model should satisfy in order to predict plastically admissible and unique response, respectively, are the following:

(a) the plastic multiplier to be non-negative during plastic flow (the condition of 'admissible plastic flow'):

$$\chi = \frac{\frac{\partial Y}{\partial \boldsymbol{\sigma}'}: \boldsymbol{C}^{el}: \dot{\boldsymbol{\varepsilon}}}{\frac{\partial Y}{\partial \boldsymbol{\sigma}'}: \boldsymbol{C}^{el}: \frac{\partial g}{\partial \boldsymbol{\sigma}'} + H} \geqslant 0, \tag{1}$$

or, alternatively, expressed in terms of the stress rates (stemming directly from the consistency condition $\dot{Y} = 0$):

$$\chi = \frac{\frac{\partial Y}{\partial \boldsymbol{\sigma}'}: \dot{\boldsymbol{\sigma}}'}{H} \geqslant 0; \tag{2}$$

(b) the denominator of the plastic multiplier in Eq. (1) to be positive at any state (the condition of 'local uniqueness'; the term is adopted after [15]):

$$\frac{\partial Y}{\partial \boldsymbol{\sigma}'}: \boldsymbol{C}^{el}: \frac{\partial g}{\partial \boldsymbol{\sigma}'} + H > 0, \tag{3}$$

where the yield function Y depends on the effective stress tensor $\boldsymbol{\sigma}'$ and the vector of internal/hardening variables $\boldsymbol{m}$, g denotes the plastic potential function, $\boldsymbol{\varepsilon}$ and $\boldsymbol{\varepsilon}^{pl}$ are the strain and plastic strain tensors, respectively, $\boldsymbol{C}^{el}$ is the elasticity tensor and H represents the plastic hardening modulus:

$$H = -\frac{1}{\chi}\left(\frac{\partial Y}{\partial \boldsymbol{m}}: \dot{\boldsymbol{m}}\right). \tag{4}$$

Assuming a linear relationship between internal variables and plastic strains, H can be simplified to

$$H = -\frac{1}{\chi}\left(\frac{\partial Y}{\partial \boldsymbol{m}}: \frac{\partial \boldsymbol{m}}{\partial \boldsymbol{\varepsilon}^{pl}}: \dot{\boldsymbol{\varepsilon}}^{pl}\right) = -\frac{\partial Y}{\partial \boldsymbol{m}}: \frac{\partial \boldsymbol{m}}{\partial \boldsymbol{\varepsilon}^{pl}}: \frac{\partial g}{\partial \boldsymbol{\sigma}'}. \tag{5}$$

The condition of local uniqueness ensures that the response of a material point is unique for any prescribed strain evolution. Eq. (3) can be derived considering the cases of plastic loading and of elastic unloading from a plastic state (see [34] and [15] for detailed derivations), and it indicates that the plastic modulus H, which is positive in the case of hardening and negative in the case of softening, should be above a certain critical value.

This can be illustrated for the simple one-dimensional case of an elasto-plastic model with linear elasticity (defined by the Young's modulus E) and linear plastic hardening (defined by the plastic modulus H), where Eq. (3) reduces to $H > -E$. Fig. 1 shows the predicted stress-strain response for several values of H qualitatively and highlights the restriction imposed by Eq. (3) on the allowable softening. Clearly, for $H < -E$, local uniqueness is violated as any solution in the zone marked grey in Fig. 1 can be obtained either from plastic loading or from elastic unloading from a plastic state. It is further worth noting that, for $H < -E$, the tangent hardening modulus ($=EH/(E + H)$) becomes positive and greater than the elastic modulus E. Therefore, plastic loading with increasing strain would generate negative plastic strain and the condition of admissible plastic flow would be violated too.

E-mail address: apostolos.vrakas@igt.baug.ethz.ch.

http://dx.doi.org/10.1016/j.compgeo.2017.09.013
Received 28 February 2017; Received in revised form 6 September 2017; Accepted 18 September 2017

Nomenclature

a	cavity radius
b	function of Poisson's ratio
$\boldsymbol{C}^{el}$	elasticity tensor
D	dilatancy function (function of η)
E	Young's modulus
f	function of η
G	shear modulus
g	plastic potential function
H	plastic hardening modulus
h	function of η
i	auxiliary index
K	bulk modulus
M	critical stress ratio (slope of the CSL in the p'–q plane)
$\boldsymbol{m}$	vector of internal variables
N	specific volume at 1 kPa on the NCL
p_{wa}	pore pressure at the cavity wall
p_{w0}	initial pore pressure
p'	mean effective stress
p'_c	isotropic preconsolidation stress
p'_e	isotropic consolidation stress at the specific volume υ
q	deviatoric stress
R	initial isotropic overconsolidation ratio
R_d	overconsolidation ratio R such that $\eta_\rho = \eta_d$
R_m	overconsolidation ratio R such that $\eta_\rho = \eta_m$
s	principal deviator stress
u_a	cavity wall displacement
Y	yield function
α	slope of a linear effective stress path in the p'–q plane
Γ	specific volume at 1 kPa on the CSL
E_p, E_q	normalized volumetric and deviatoric strain
$\boldsymbol{\varepsilon}$	strain tensor
ε_a, ε_r	axial and radial strain
ε_p, ε_q	volumetric and deviatoric strain
ε_1, ε_2, ε_3	major, intermediate and minor principal strain
η	stress ratio q/p'
η_d	critical stress ratio η for ensuring uniqueness under pure strain control
η_m	critical stress ratio η for ensuring uniqueness under mixed stress-strain control
κ, λ	slope of URL and NCL in the ln p'–υ plane
Λ	$=1-\kappa/\lambda$
ν	Poisson's ratio
σ_a	total radial stress at the cavity wall
σ_0	initial isotropic total stress
$\boldsymbol{\sigma'}$	effective stress tensor
σ'_a, σ'_r	axial and radial effective stress
σ'_1, σ'_2, σ'_3	major, intermediate and minor principal effective stress
υ	specific volume
χ	plastic multiplier

Subscripts

0	initial value
cs	value at critical state
ρ	value at yielding

Superscripts

el	elastic part
pl	plastic part

This simple example shows that there is a limit on the allowable softening of an elasto-plastic model. When this limit is exceeded, the predicted response is not admissible. This paper investigates this limit for the modified Cam-clay (MCC) model [29].

The MCC model is the most widely-used critical state constitutive model in the analysis of geotechnical problems. It is developed within the classic framework of critical state theory [30,31], according to which, after a certain amount of shearing, the material reaches a critical state, defined as the state where the material continues deforming in shear under constant volume and effective stresses. When yielding occurs on the 'wet' (or subcritical) side, the post-yield response involves strain-hardening, while when yielding occurs on the 'dry' (or supercritical) side, the post-yield response involves strain-softening. The MCC model is reasonably good at reproducing the behaviour of normally and slightly overconsolidated soils which exhibit 'wet' behaviour'. Its deficiencies for heavily overconsolidated soils which exhibit 'dry' behaviour (for example, the overestimation of yield stresses, *e.g.* [13,17], or the assumption of elastic response inside the state boundary surface, *e.g.* [36]) are known and addressed by refined models (see among others reviews by [26,1,39]), but MCC model remains the most widely-used critical state model over the entire range of initial conditions.

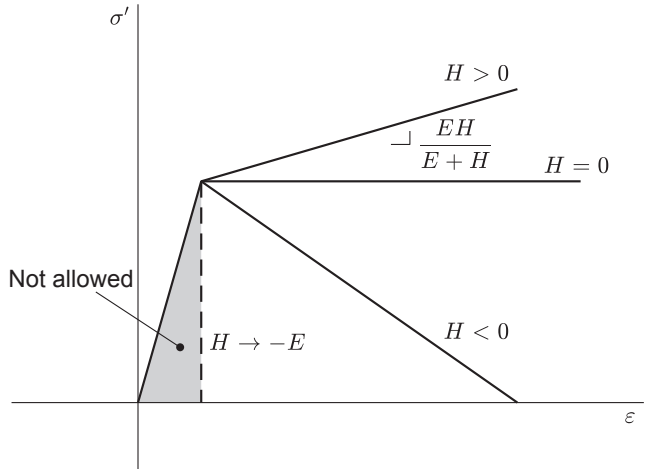

Fig. 1. One-dimensional stress-strain response according to an elasto-plastic model with linear hardening; limit on the allowable softening after Eq. (3) (figure modified from [34]).

In the numerical analysis of geotechnical problems, the occurrence of high overconsolidation ratios is inevitable (at least in part of the model). For example, the application of a relatively small preconsolidation pressure at the ground surface in order to define the initial state of a slightly overconsolidated soil layer leads to very high overconsolidation ratios in its upper part where the *in situ* stresses are low. Therefore, the computational applicability of the MCC model on the 'dry' side is particularly relevant for geotechnical applications. Since the model was first proposed by Roscoe and Burland [29], it has been used and implemented extensively (*e.g.* [40,20,5,10,6,7,11,25,33,27,35]), and is meticulously described nowadays in almost all geomechanics textbooks (*e.g.* [3,18,24,28]). To the author's knowledge, however, there is no work dealing with its computational applicability on the 'dry' side. This forms a gap in the understanding of the limits of the MCC model in analyses of boundary value problems, and it has motivated the present paper.

The paper starts with a brief presentation of the MCC model (Section 2), continuing with a theoretical investigation into the allowable softening for ensuring local uniqueness in arbitrary strain-controlled loadings (Section 3) and in the basic drained and undrained triaxial loadings (Section 4) and closing with a discussion of the

implications in the numerical analysis of boundary value problems (Section 5).

2. The modified Cam-clay model

The MCC model involves five material parameters: (a) the Poisson's ratio ν (or the shear modulus G); (b) the slope κ of the unloading-reloading line (URL; $\dot{v} = -\kappa\dot{p}'/p'$) and (c) the slope λ of the normal consolidation line (NCL; $\dot{v} = -\lambda\dot{p}'/p'$) in the ln p'–v plane, where p' is the mean effective stress and v is the specific volume; (d) the slope M of the critical state line (CSL) in the p'–q plane, where q is the deviatoric stress; and (e) the ordinate Γ of the CSL in the ln p'–v plane at unit reference pressure (or the ordinate N of the NCL; since the MCC model assumes a constant spacing ratio between the CSL and the NCL equal to 2, $N = \Gamma + (\lambda-\kappa)\ln 2$). A general small-strain formulation of the two-invariant MCC model is presented in the following.

2.1. General constitutive equations

Considering a plastic potential $g(p', q)$ and using Hooke's law for the elastic part (denoted by the superscript '*el*') and the flow rule for the plastic part (denoted by the superscript '*pl*'), the set of constitutive equations in the principal stress space can be written as follows:

$$\dot{\varepsilon}_i = \dot{\varepsilon}_i^{el} + \dot{\varepsilon}_i^{pl} = \frac{\dot{p}'}{3K} + \frac{\dot{s}_i}{2G} + \chi\left(\frac{1}{3}\frac{\partial g}{\partial p'} + \frac{3s_i}{2q}\frac{\partial g}{\partial q}\right), \tag{6}$$

where $i = 1,2,3$, $\dot{\varepsilon}_i$ is the strain rate, K and G are the elastic bulk and shear modulus, respectively, χ is the plastic multiplier, $s_i = \sigma'_i - p'$ and

$$p' = \frac{\sigma'_1 + \sigma'_2 + \sigma'_3}{3}, \tag{7}$$

$$q = \sqrt{\frac{(\sigma'_1-\sigma'_2)^2 + (\sigma'_2-\sigma'_3)^2 + (\sigma'_3-\sigma'_1)^2}{2}}. \tag{8}$$

Compressive stresses (and strains) are taken as positive with $\sigma'_3 < \sigma'_2 < \sigma'_1$. Defining the generalised strain rates as

$$\dot{\varepsilon}_p = \dot{\varepsilon}_1 + \dot{\varepsilon}_2 + \dot{\varepsilon}_3, \tag{9}$$

$$\dot{\varepsilon}_q = \frac{s_1\dot{\varepsilon}_1 + s_2\dot{\varepsilon}_2 + s_3\dot{\varepsilon}_3}{q}, \tag{10}$$

the constitutive equations can be transformed in the p'–q stress space to:

$$\dot{\varepsilon}_p = \dot{\varepsilon}_p^{el} + \dot{\varepsilon}_p^{pl} = \frac{\dot{p}'}{K} + \chi\frac{\partial g}{\partial p'}, \tag{11}$$

$$\dot{\varepsilon}_q = \dot{\varepsilon}_q^{el} + \dot{\varepsilon}_q^{pl} = \frac{\dot{q}}{3G} + \chi\frac{\partial g}{\partial q}. \tag{12}$$

2.2. Elasticity

Pressure dependent elastic stiffness is assumed with a constant Poisson's ratio. Although this assumption leads to a non-conservative (hypo-elastic) model [41,12], it is used widely, being regarded as sufficient for monotonic/static loadings. It is preferred here over the assumption of a constant shear modulus (which leads to a conservative model) in order to keep all the material parameters dimensionless. (Section 4.1 deals with the problem of shear loading under constant mean effective stress, verifying that the assumption of a constant shear modulus is not essential for the outcome of the paper.)

The elastic bulk and shear modulus are then equal to (*e.g.* [18]; note that according to small strain theory $\dot{\varepsilon}_p = -\dot{v}/v_0$, where v_0 denotes the initial specific volume)

$$K = \frac{v_0}{\kappa}p', \tag{13}$$

$$G = \frac{K}{3b}, \quad b = \frac{2(1+\nu)}{9(1-2\nu)}. \tag{14}$$

2.3. Yield function, plastic potential and hardening law

The yield function of the MCC reads as follows:

$$Y(p', q, p'_c) = \frac{M^2 + \eta^2}{M^2} - \frac{p'_c}{p'} = 0, \tag{15}$$

where the stress ratio $\eta = q/p'$ and p'_c is the preconsolidation pressure, denoting the mean effective stress at $\eta = 0$ and acting as the hardening parameter, as it defines the size of the yield surface.

The model assumes associated plastic flow ($g = Y$), and the stress-dilatancy relation equals

$$\frac{\dot{\varepsilon}_p^{pl}}{\dot{\varepsilon}_q^{pl}} = D(\eta) = \frac{M^2-\eta^2}{2\eta}. \tag{16}$$

The dilatancy function D vanishes at critical state, *i.e.* $D(M) = 0$, leading to zero plastic volumetric deformations, while it tends to infinity for isotropic loadings, *i.e.* $D(0) = \infty$.

Hardening is attributed solely to accumulated plastic volumetric strains and thus the hardening law is expressed as follows (*e.g.* [18]):

$$\frac{\dot{p}'_c}{p'_c} = \frac{v_0}{\lambda-\kappa}\dot{\varepsilon}_p^{pl}. \tag{17}$$

2.4. Stress-strain relationship

The plastic multiplier can be determined from the consistency condition, namely

$$\dot{Y} = \frac{\partial Y}{\partial p'}\dot{p}' + \frac{\partial Y}{\partial q}\dot{q} + \frac{\partial Y}{\partial p'_c}\dot{p}'_c = 0, \tag{18}$$

the hardening law (Eq. (17)) and the differential $\dot{q} = \eta\dot{p}' + p'\dot{\eta}$ (*cf.* Eq. (2)):

$$\chi = \frac{\frac{\dot{p}'}{p'} + \frac{2\eta}{M^2+\eta^2}\dot{\eta}}{\frac{M^2-\eta^2}{p'M^2}\frac{v_0}{\lambda-\kappa}}. \tag{19}$$

Therefore, the elasto-plastic constitutive Eqs. (11) and (12), with the aid of Eq. (19) and the strain normalization $E_i = \varepsilon_i \cdot (v_0/\kappa)$, lead to:

$$\begin{Bmatrix}\dot{E}_p\\ \dot{E}_q\end{Bmatrix} = \begin{bmatrix}\lambda/\kappa & \frac{(\lambda/\kappa-1)2\eta}{M^2+\eta^2}\\ b\eta + \frac{(\lambda/\kappa-1)2\eta}{M^2-\eta^2} & b + \frac{(\lambda/\kappa-1)4\eta^2}{M^4-\eta^4}\end{bmatrix}\begin{Bmatrix}\dot{p}'/p'\\ \dot{\eta}\end{Bmatrix}. \tag{20}$$

The above compliance matrix depends on a single state variable: the stress ratio η.

The plastic multiplier can also be determined in terms of strain rates, using the consistency condition (18), the hardening law (Eq. (17)) and Eqs. (11), (12) (*cf.* Eq. (1)):

$$\chi = \frac{\frac{\partial Y}{\partial p'}K\dot{\varepsilon}_p + \frac{\partial Y}{\partial q}3G\dot{\varepsilon}_q}{\left(\frac{\partial Y}{\partial p'}\right)^2 K + \left(\frac{\partial Y}{\partial q}\right)^2 3G - \frac{\partial Y}{\partial p'_c}\frac{v_0}{\lambda-\kappa}p'_c\frac{\partial Y}{\partial p'}} = \frac{\left(\frac{M^2-\eta^2}{M^2}\right)\dot{E}_p + \frac{2\eta}{bM^2}\dot{E}_q}{\frac{v_0}{\kappa p'}h(\eta)}, \tag{21}$$

where

$$h(\eta) = \left(1-\frac{1}{\lambda/\kappa-1}\right)\left(\frac{\eta}{M}\right)^4 - 2\left(1-\frac{2}{bM^2}\right)\left(\frac{\eta}{M}\right)^2 + 1 + \frac{1}{\lambda/\kappa-1} > 0. \tag{22}$$

Substituting Eq. (21) into Eqs. (11) and (12) leads to the inverse (of Eq. (20)) constitutive relationship. However, Eq. (20) facilitates the following theoretical analysis.

2.5. Critical state and state boundary surface

The critical state (denoted by the subscript '*cs*') is defined by the following conditions [31]:

$$p'_{cs} = \exp[(\Gamma - \upsilon_{cs})/\lambda], \quad q_{cs} = M p'_{cs}. \tag{23}$$

Finally, the yield function in combination with the semi-logarithmic compression laws (which, after simple geometric considerations, imply $p'_c = (p'_e/p')^{1/\Lambda} p'$, where $p'_e = \exp[(N-\upsilon)/\lambda]$ is the mean effective stress on the NCL at the current specific volume and $\Lambda = 1 - \kappa/\lambda$) produces the state boundary surface (SBS) in the p'–q–υ space:

$$\left(\frac{p'}{p'_e}\right)^{-1/\Lambda} - \left(\frac{\eta}{M}\right)^2 - 1 = 0. \tag{24}$$

The SBS separates possible from impossible states [31,3]. Specifically, for states inside the SBS the material behaviour is elastic, for states on the SBS the material behaviour is elasto-plastic, and states outside the SBS cannot exist. The concept of a unique SBS, which implies that any monotonous loading path moves (after yielding) on this single SBS until terminating on the CSL, is fundamental to the framework of classic critical state theory.

Eq. (24) shows that for any constant υ section in the p'–q–υ space (p'_e = const.), the shape of the SBS remains the same, although its size is different. It is convenient therefore to consider a two-dimensional representation by normalizing the stresses to the pressure p'_e. Fig. 2 plots the SBS in the $p'/p'_e - q/p'_e$ plane for various values of the slope ratio κ/λ and $M = 1$. As can be seen, for κ/λ greater than 0.5 the SBS is not convex on the 'dry' side, with the deviatoric stress tending to infinity as the mean effective stress tends to zero. Although κ/λ typically varies for soils between 0.1 and 0.4, values greater than 0.5 may generally be used; for example, Sheng and Sloan [32] considered $\kappa/\lambda = 0.6$ for a medium density sand. Moreover, there are cases where the parameter values are selected so that the MCC model can better predict specific experimentally observed stress-strain relationships and are thus released from their physical origins; for example, Muir Wood et al. [19] showed that κ/λ should be up to 0.77 in order to improve the MCC predictions for the deviatoric stress-strain response of a kaolin specimen subject to constant p' loading. Finally, these high values of κ/λ are required so that the MCC model will not over-predict the measured values for the coefficient of earth pressure at rest in respect of normally consolidated clays [29,9]. Consequently, a κ/λ ratio greater than 0.5 can be considered in computational applications.

3. Theoretical investigation into the allowable softening for ensuring local uniqueness in arbitrary strain-controlled loadings

Local uniqueness is satisfied as long as the denominator of the plastic multiplier in Eq. (21), and thus the function h (Eq. (22)), remains positive. As the function h depends only on the material constants and on the current stress state, it can be evaluated independently of the loading path. The smallest positive root of the quadratic equation $h(\eta) = 0$ reads as follows:

$$\frac{\eta_d}{M} = \sqrt{\frac{1 - \frac{2}{bM^2} - \sqrt{\left(1 - \frac{2}{bM^2}\right)^2 - 1 + \left(\frac{1}{\lambda/\kappa - 1}\right)^2}}{1 - \frac{1}{\lambda/\kappa - 1}}}, \tag{25}$$

while in the special case that $\kappa/\lambda = 0.5$:

$$\frac{\eta_d}{M} = \sqrt{1 \Big/ \left(1 - \frac{2}{bM^2}\right)}. \tag{26}$$

For stress ratios greater than η_d the function h becomes negative. This is shown in Fig. 3, which plots the function h for $\nu = 0.35$, $M = 1$ and three values of the κ/λ ratio: for $\kappa/\lambda = 0.4$ and 0.5 the function remains always positive, while for $\kappa/\lambda = 0.6$ it becomes negative beyond $\eta_d = 2.24$. Therefore, η_d denotes the critical (maximum allowable) stress ratio for ensuring local uniqueness and holds for any arbitrary strain-controlled loading path.

Fig. 4 shows the normalized stress ratio η_d as a function of the critical stress ratio M for several values of the Poisson's ratio ν and $\kappa/\lambda = 0.5$ and 0.6. As can be seen, the higher the slope ratio, the Poisson's ratio and the critical stress ratio, the lower the normalized ratio η_d/M. More specifically, for $\kappa/\lambda = 0.5$, uniqueness is practically always satisfied up to $\nu = 0.35$; for $\kappa/\lambda > 0.5$, uniqueness can be violated at relatively low stress ratios; while for the most common and realistic case that $\kappa/\lambda < 0.5$, uniqueness problems do not exist (they are encountered only at unrealistically high values of the Poisson's ratio, where b increases asymptotically; note that according to Eqs. (25) and (26) η_d/M approaches unity as b tends to infinity).

Therefore, it can be concluded that the MCC model satisfies the standard condition of local uniqueness (Eq. (3)) in most cases, with the exception of some less typical ones. However, this is not true for the condition of local uniqueness under mixed stress- and strain-controlled loading conditions, which will be shown in the following to be violated for typical parameter sets.

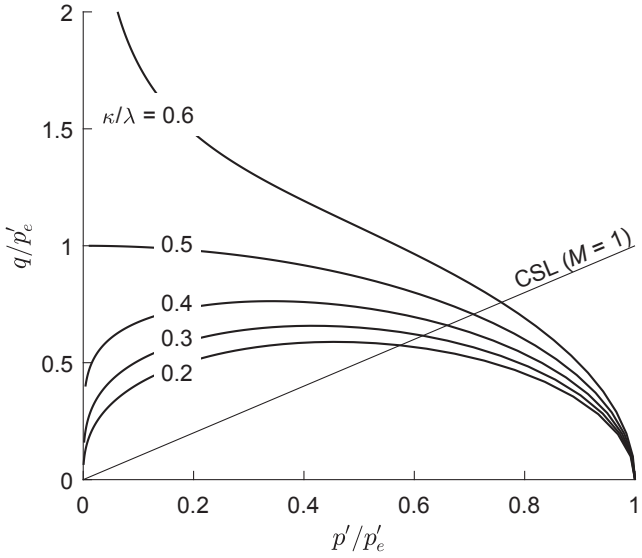

Fig. 2. State boundary surfaces in the p'/p'_e–q/p'_e plane.

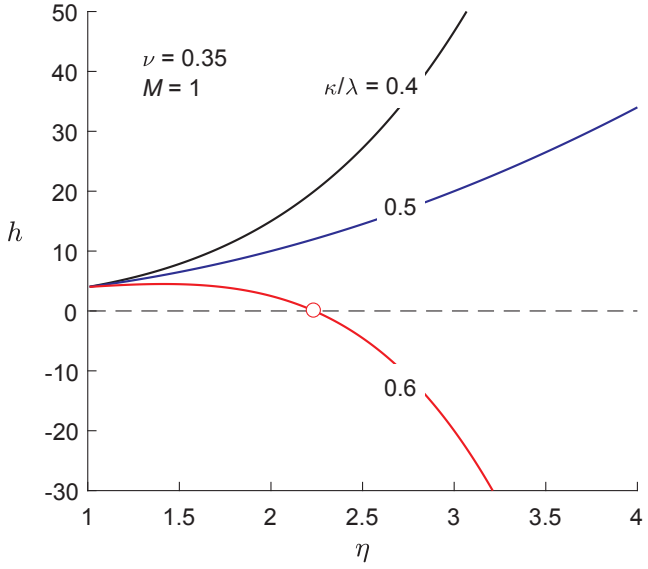

Fig. 3. Representation of the function h (Eq. (22)).

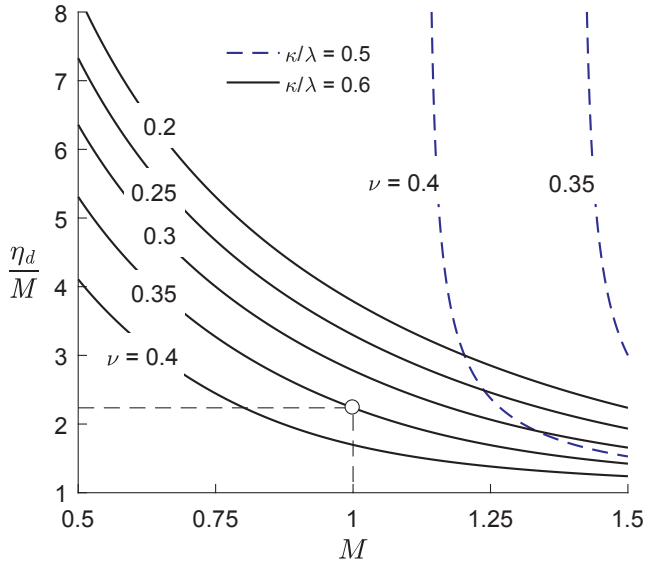

Fig. 4. Normalized critical stress ratio η_d for ensuring local uniqueness as a function of the critical stress ratio M for several values of the Poisson's ratio ν and the slope ratio κ/λ.

4. Theoretical investigation into the allowable softening for ensuring local uniqueness in triaxial compression loadings

The following sections investigate the condition of local uniqueness for all the basic triaxial loadings. The stress and strain rate parameters (Eqs. (7)–(10)) then simplify to

$$p' = \frac{\sigma'_a + 2\sigma'_r}{3}, \quad q = |\sigma'_a - \sigma'_r|, \tag{27}$$

$$\dot{\varepsilon}_p = \dot{\varepsilon}_a + 2\dot{\varepsilon}_r, \quad \dot{\varepsilon}_q = \frac{2}{3}|\dot{\varepsilon}_a - \dot{\varepsilon}_r|, \tag{28}$$

where σ'_a and σ'_r denote the axial and radial effective stresses and ε_a and ε_r denote the corresponding strains.

In the case of triaxial compression, where the axial direction is the major principal direction, the normalized axial strain rate can be expressed with respect to the strain rate invariants as follows:

$$\dot{E}_1 = \dot{E}_a = \dot{E}_p/3 + \dot{E}_q. \tag{29}$$

Substitution of the volumetric and deviatoric strains from Eq. (20) into Eq. (29) indicates that for any prescribed monotonously increasing strain evolution the following condition should be satisfied:

$$\dot{E}_1 = \left[\frac{\lambda/\kappa}{3} + b\eta + \frac{(\lambda/\kappa - 1)2\eta}{M^2 - \eta^2}\right]\frac{\dot{p}'}{p'} + \left[b + \frac{(\lambda/\kappa - 1)2\eta}{M^2 + \eta^2}\left(\frac{1}{3} + \frac{2\eta}{M^2 - \eta^2}\right)\right]\dot{\eta} \quad > \quad 0. \tag{30}$$

Provided that the current mean effective stress p' can be expressed as a function of the current stress ratio η under triaxial loading conditions (as will be proved in the next sections), Eq. (30) can be generalized to:

$$\dot{E}_1 = f(\eta)\dot{\eta} \quad > \quad 0, \tag{31}$$

where for given stress path and material constants the function f depends solely on the current stress ratio η. According to the MCC model, after yielding on the 'wet' side, η should increase up to the critical stress ratio M, which implies $\dot{\eta} > 0$ and thus $f(\eta) > 0$, while, after yielding on the 'dry' side, η should decrease down to the critical stress ratio M, which implies $\dot{\eta} < 0$ and thus $f(\eta) < 0$. However, the latter condition is not always satisfied. As will be shown in the following, there is a critical stress ratio, denoted by η_m, beyond which the function f becomes positive.

Provided that first yielding occurs at $\eta > \eta_m$ (point A in Fig. 5), this means that: (a) in a strain-controlled loading process (*i.e.* $\dot{E}_1 > 0$), η will not decrease down to the critical stress ratio M after yielding but will increase indefinitely (since $\dot{\eta} > 0$ after Eq. (31); dashed curve A-C in Fig. 5), thus leading to a negative plastic multiplier (see Eq. (19)); while (b) in a stress-controlled loading process (*i.e.* for decreasing stress ratio or deviatoric stress after yielding, $\dot{\eta} < 0$), the stress-strain curve will present a 'snap-back', that is, the axial strain will decrease (as long as f remains positive, according to Eq. (31); solid curve A-A′ in Fig. 5) and then increase again (from the point that f becomes negative; solid curve A′-B in Fig. 5), with the plastic multiplier always remaining positive (see Eq. (19)). For this reason η_m will be referred in the following as the 'snap-back threshold' (this term was inspired by [4]). In the post-yield region where the axial strain decreases (A-A′ in Fig. 5), the response is not unique in terms of the stress ratio η. More specifically, there are two possible solutions: one corresponding to plastic loading and one corresponding to elastic unloading from a plastic state.

Consequently, local uniqueness is lost at $\eta = \eta_m$, where $\eta_m \leq \eta_d$ (see next sections). The fact that the loading path affects the condition of local uniqueness – and thus the value of η_m here – is already known in the literature. Specifically, Klisinski et al. [16], Nova [21] and Imposimato and Nova [14] have shown that the critical plastic hardening modulus for ensuring uniqueness is lower in tests under mixed control (*i.e.* combined stress and strain control, as for example in conventional triaxial compression tests where the confining stress is kept constant and the axial strain increases) than in tests under pure strain control.

The function f and the overall model behaviour will be studied in the following for the main triaxial compression loadings (Sections 4.1–4.3). Some representative results for the corresponding triaxial extension loadings are given in the Appendix A. The material constants used are typical of a clayey material, but do not correspond to any particular soil (see Table 1): $\nu = 0.35$ ($b = 1$), $\kappa/\lambda = 0.4$ (*e.g.* London clay; [31]) with $\kappa = 0.02$, $M = 1$ (*i.e.* the friction angle varies from $\sim 25^\circ$ in triaxial compression to $\sim 35^\circ$ in triaxial extension) and $\Gamma = 2.5$. The standard condition of local uniqueness is always satisfied for this parameter set ($\eta_d \to \infty$). Only in the case of undrained loading does the slope ratio have to be increased (κ/λ is set to 0.6) for reasons explained later. The initial preconsolidation pressure p'_{c0} is taken equal to 1000 kPa. Although the following theoretical analysis is valid for arbitrary initial stress states, the paper as a whole considers only isotropic states (*i.e.* $q_0 = 0$) for the sake of simplicity.

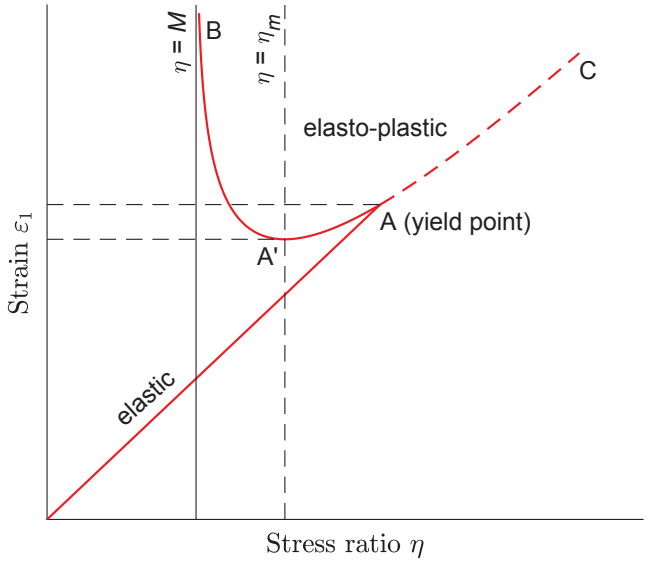

Fig. 5. Schematic representation of triaxial response for $\eta > \eta_m$: stress ratio vs. axial strain.

Table 1
Model parameters and uniqueness thresholds for the triaxial compression load cases analysed.

Load case	ν	κ	κ/λ	M	Γ	p'_{c0} [kPa]	$R = p'_{c0}/p'_0$	η_m	R_m
Constant p'	0.35	0.02	0.4	1.0	2.5	1000	1.5/5/10	2.13	5.55
Drained loading	0.35	0.02	0.4	1.0	2.5	1000	1.5/10/20	1.88	12.13
Drained unloading	0.35	0.02	0.4	1.0	2.5	1000	1/2/4	2.89	3.19
Undrained	0.35	0.02	0.6	1.0	2.5	1000	1.5/5/7	2.24	6.00

4.1. Load case 1: Constant p' loading

4.1.1. Governing equations

The simplest case of shear loading under constant mean effective stress (*e.g.* [38,19]) is analysed first, because it allows the derivation of simple closed-form relationships that facilitate understanding of the model behaviour. Shearing under constant mean effective stress implies a vertical stress path in the p'–q plane, starting from the initial stress state (p'_0, q_0) (denoted by the subscript '0' and indicated by circular marks; Fig. 6a). The response is linearly elastic until the yield surface is reached and then becomes elasto-plastic. The conditions at yielding (denoted by the subscript 'ρ' and indicated by triangular marks; Fig. 6a) read as follows:

$$\eta_\rho = M\sqrt{R-1}, \tag{32}$$

$$E_{q\rho} = b(\eta_\rho - \eta_0), \tag{33}$$

where η_0 is the initial stress ratio ($=q_0/p'_0$) and R is the initial isotropic overconsolidation ratio (defined as the ratio of p'_{c0} to p'_0). The integration of Eq. (20) over the elasto-plastic stress history gives

$$E_p(\eta) = \ln\left[\left(\frac{\eta^2+M^2}{\eta_\rho^2+M^2}\right)^{\lambda/\kappa-1}\right], \tag{34}$$

$$E_q(\eta) = E_{q\rho} + b(\eta-\eta_\rho) + \frac{\lambda/\kappa-1}{M}\times\left\{\ln\left[\frac{(\eta+M)(\eta_\rho-M)}{(\eta-M)(\eta_\rho+M)}\right] -2\left[\tan^{-1}\left(\frac{\eta}{M}\right)-\tan^{-1}\left(\frac{\eta_\rho}{M}\right)\right]\right\}. \tag{35}$$

According to Eq. (30), the following condition should be satisfied on the 'dry' side:

$$f(\eta) = b + \frac{(\lambda/\kappa-1)2\eta}{M^2+\eta^2}\left(\frac{1}{3}+\frac{2\eta}{M^2-\eta^2}\right) \quad < \quad 0. \tag{36}$$

However, the sign of function f for $\eta > M$ depends on the values of the material constants and the current stress ratio. Fig. 7 plots the function f for the parameter set considered (black curve) and verifies that it becomes positive beyond $\eta_m = 2.13$. Although the (first positive) root η_m of the equation $f(\eta) = 0$ cannot be determined analytically, it can be determined by means of a standard Newton's scheme. The

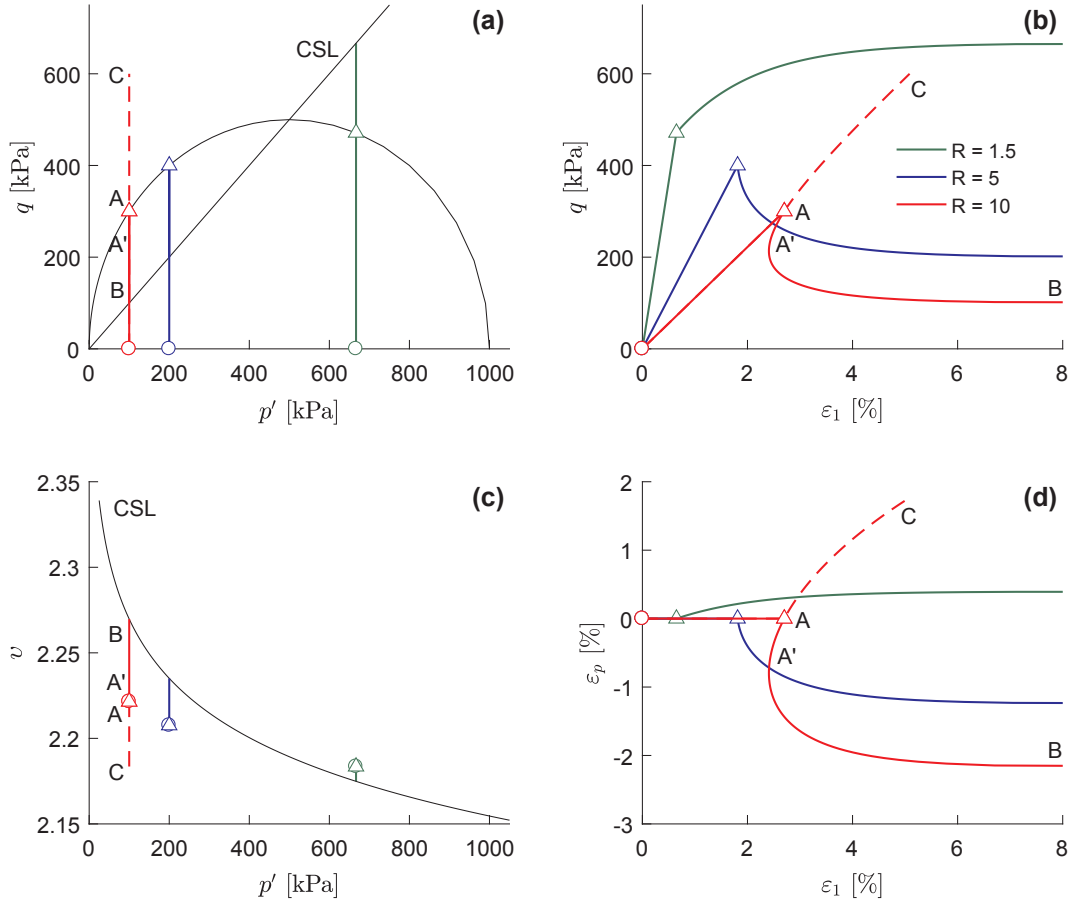

Fig. 6. MCC model predictions for the constant p' loading test: (a) mean effective stress vs. deviatoric stress; (b) axial strain vs. deviatoric stress; (c) mean effective stress vs. specific volume and; (d) axial strain vs. volumetric strain.

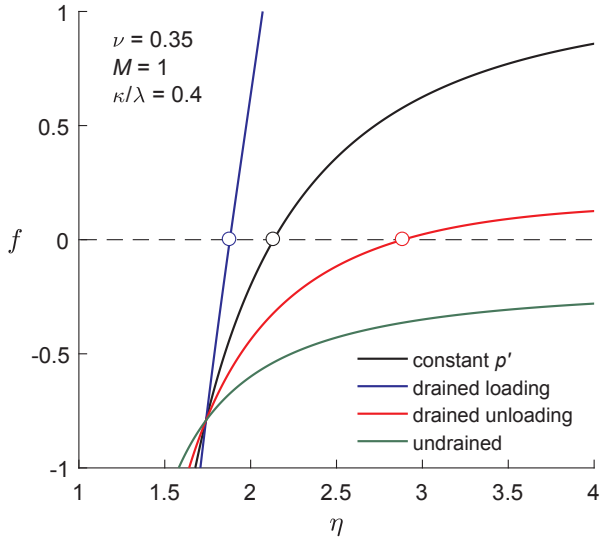

Fig. 7. Representation of the function f for four triaxial compression cases: constant p' loading (Eq. (36)); drained loading, $\alpha = 3$ (Eq. (45)); drained unloading, $\alpha = -3/2$ (Eq. (45)); undrained loading (Eq. (50)).

condition that $\eta < \eta_m$ then imposes, together with Eq. (32), the following restriction on the overconsolidation ratio:

$$R < R_m = 1 + (\eta_m/M)^2, \tag{37}$$

where R_m denotes the overconsolidation ratio R such that $\eta_p = \eta_m$ (that is, the maximum allowable overconsolidation ratio while not exceeding the snap-back threshold at yielding).

Fig. 8 shows (a) the normalized stress ratio η_m and (b) the corresponding overconsolidation ratio R_m as a function of the critical stress ratio M for some typical values of the Poisson's ratio and the slope ratio κ/λ. The results reveal that the snap-back threshold values can be very low, decreasing with the material constants M, ν and κ/λ; for the present parameter set R_m equals 5.55 (marked point in Fig. 8b). Moreover, it should be pointed out that the snap-back threshold exists in cases where the standard condition of local uniqueness is satisfied. A specific example is analysed in detail in the following in order to illustrate the model behaviour when η_m is exceeded.

4.1.2. Model predictions

Three cases are chosen for the overconsolidation ratio: (a) $R = 1.5$ (yielding on the 'wet' side); (b) $R = 5$ (yielding on the 'dry' side; Eq. (37) is satisfied) and; (c) $R = 10$ (yielding on the 'dry' side; Eq. (37) is violated). Note for completeness that the elastic response remains linear here and therefore a formulation based on a constant shear modulus equal to $K/3$ (since $b = 1$) would be totally equivalent.

Fig. 6 presents the predicted triaxial response for the three cases considered. According to the expected model behaviour, after first yielding, η increases up to the critical stress ratio M in the first case (green curve in Fig. 6a and b), and decreases down to the critical stress ratio M in the second case (blue curve in Fig. 6a and b). At the same time, the material contracts and dilates, respectively, till critical state conditions are reached (Fig. 6c and d).

This is not the case for $R = 10$, where, after first yielding (point A), the aforementioned 'snap-back' response takes place for decreasing deviatoric stress (*i.e.* stress-controlled loading). Specifically, the axial strain decreases and increases again (red solid curves in Fig. 6b and d) until critical state conditions are reached (point B). It is worth noting that the plastic multiplier always remains positive according to Eq. (19).

Nevertheless, the predicted response is plastically inadmissible for increasing axial strain (*i.e.* strain-controlled loading). After the results from the stress-controlled loading (red solid curves A-A′-B in Fig. 6), it might be expected that the post-yield response presents a discontinuity, with a negative jump in deviatoric stress and volumetric strain. What actually happens, however, is the following: with increasing axial strain, the stress ratio increases (and the deviatoric stress increases too) and the material constantly contracts (dashed red curves in Fig. 6). Therefore, the predicted stress path A-C departs from rather than moves towards the CSL, which contradicts the basic principle of critical state theory. It is emphasized that contraction on the 'dry' side involves negative plastic strains as the plastic multiplier becomes negative (according to Eq. (19); note that in Eq. (21) the nominator becomes negative).

The predicted inadmissible response is explained as follows. Fig. 9 plots the axial strain as a function of the stress ratio η for the three cases considered. The stress ratio η_m corresponds to the minimum of the post-yield curves on the 'dry' side (since f is the derivative of ε_1; Eq. (31)). In the third case ($R = 10$), the stress ratio at first yielding (triangular red mark; point A) is to the right of the turning point and therefore, with increasing strain, the response follows the red dashed path A-C (where η increases) and not the red solid path A-A′-B (where η decreases). It is repeated that uniqueness with respect to η is violated in the post-yield region A-A′ where the axial strain decreases.

4.2. Load case 2: Drained loading under a linear effective stress path

4.2.1. Governing equations

The second case analysed concerns the drained loading under the

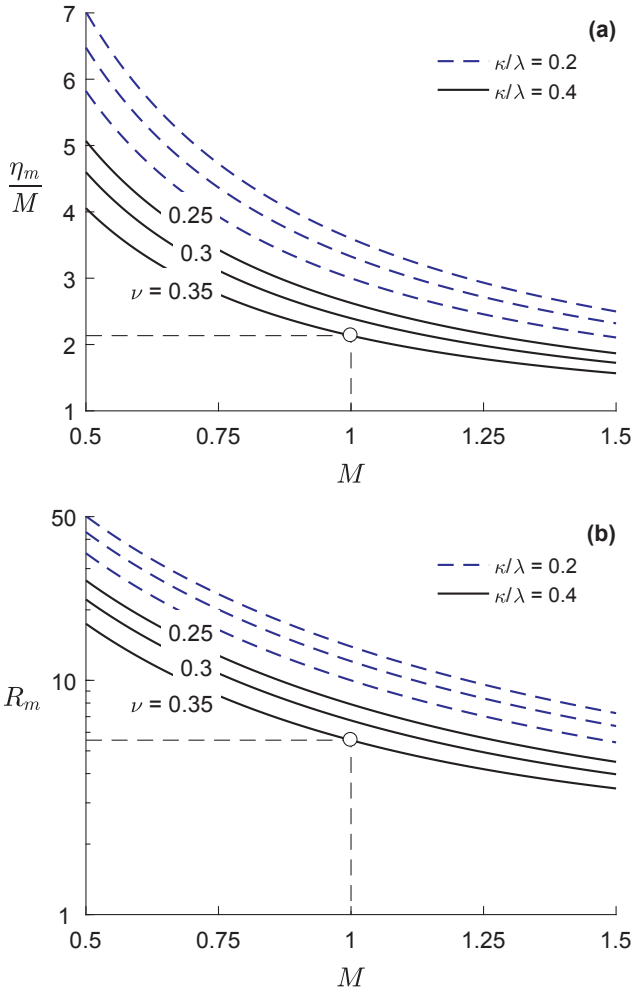

Fig. 8. (a) Normalized snap-back threshold η_m and (b) maximum allowable overconsolidation ratio R_m as a function of the critical stress ratio M for several values of the Poisson's ratio ν and the slope ratio κ/λ, in the case of constant p' loading with $\sigma'_a = \sigma'_1$.

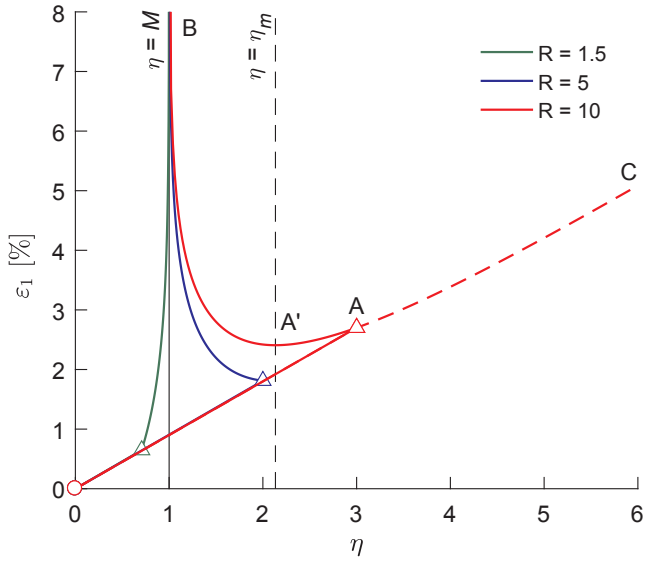

Fig. 9. Axial strain as a function of the stress ratio η for the constant p' loading test (example in Fig. 6).

linear effective stress path of slope α in the p'–q plane (*i.e.* $\alpha = \dot{q}/\dot{p}'$), which implies together with the differential $\dot{q} = \eta\dot{p}' + p'\dot{\eta}$:

$$\frac{\dot{p}'}{p'} = \frac{\dot{\eta}}{\alpha - \eta}. \tag{38}$$

Integrating Eq. (38) over the elastic domain,

$$p'_\rho = \frac{\alpha - \eta_0}{\alpha - \eta_\rho} p'_0, \tag{39}$$

and inserting it into the yield function leads to the following relation (note that $R = p'_{c0}/p'_0$):

$$R = \frac{\eta_\rho^2 + M^2}{M^2} \frac{\alpha - \eta_0}{\alpha - \eta_\rho}. \tag{40}$$

The conditions at yielding therefore read as follows:

$$\eta_\rho = \frac{M^2}{2(\alpha - \eta_0)} \left\{ \pm \sqrt{R^2 + \frac{4(\alpha - \eta_0)[\alpha(R-1) + \eta_0]}{M^2}} - R \right\}, \tag{41}$$

where the upper sign holds for $\alpha > 0$ and the lower sign holds for $\alpha < 0$; and

$$E_{p\rho} = \frac{E_{q\rho}}{\alpha b} = \ln\left(\frac{\alpha - \eta_0}{\alpha - \eta_\rho}\right). \tag{42}$$

Integration of Eq. (20) leads to (see also [22])

$$E_p(\eta) = E_{p\rho} + \ln\left[\left(\frac{\alpha - \eta}{\alpha - \eta_\rho}\right)^{-\lambda/\kappa} \left(\frac{\eta^2 + M^2}{\eta_\rho^2 + M^2}\right)^{\lambda/\kappa - 1}\right], \tag{43}$$

$$E_q(\eta) = E_{q\rho} - \ln\left[\left(\frac{\alpha - \eta}{\alpha - \eta_\rho}\right)^{\alpha\left(b + 2\frac{\lambda/\kappa - 1}{M^2 - \alpha^2}\right)}\right] + \frac{\lambda/\kappa - 1}{M} \times \left\{ \ln\left[\left(\frac{\eta + M}{\eta_\rho + M}\right)^{\alpha/(M+\alpha)} \left(\frac{\eta - M}{\eta_\rho - M}\right)^{\alpha/(M-\alpha)}\right] - 2\left[\tan^{-1}\left(\frac{\eta}{M}\right) - \tan^{-1}\left(\frac{\eta_\rho}{M}\right)\right] \right\}. \tag{44}$$

According to Eqs. (30) and (38), the following condition should be satisfied on the 'dry' side:

$$f(\eta) = \left[\frac{\lambda/\kappa}{3} + b\eta + \frac{(\lambda/\kappa - 1)2\eta}{M^2 - \eta^2}\right] \frac{1}{\alpha - \eta} + b + \frac{(\lambda/\kappa - 1)2\eta}{M^2 + \eta^2} \left(\frac{1}{3} + \frac{2\eta}{M^2 - \eta^2}\right) < 0. \tag{45}$$

Similarly to the case of constant p' loading, the equation $f(\eta) = 0$ cannot be solved with respect to η analytically and therefore the snap-back threshold η_m has to be calculated numerically. Fig. 7 plots the function f for the special cases of conventional triaxial compression ($\alpha = 3$; blue curve) and triaxial compression under constant axial stress and decreasing confining pressure ($\alpha = -3/2$; red curve) and shows that the inequality (45) is not satisfied for stress ratios greater than 1.88 and 2.89, respectively, where f becomes positive.

The overconsolidation ratio should then satisfy the following restriction (after Eq. (40)):

$$R < R_m = \frac{\eta_m^2 + M^2}{M^2} \frac{\alpha - \eta_0}{\alpha - \eta_m}, \tag{46}$$

where R_m also depends on the initial stress ratio η_0 here, but, as mentioned earlier, only isotropic states are considered in the applications for the sake of simplicity. Figs. 10 and 11 show for these two triaxial compression cases (a) the normalized stress ratio η_m and (b) the corresponding overconsolidation ratio R_m (for $\eta_0 = 0$) as a function of the critical stress ratio M for some typical values of the Poisson's ratio and

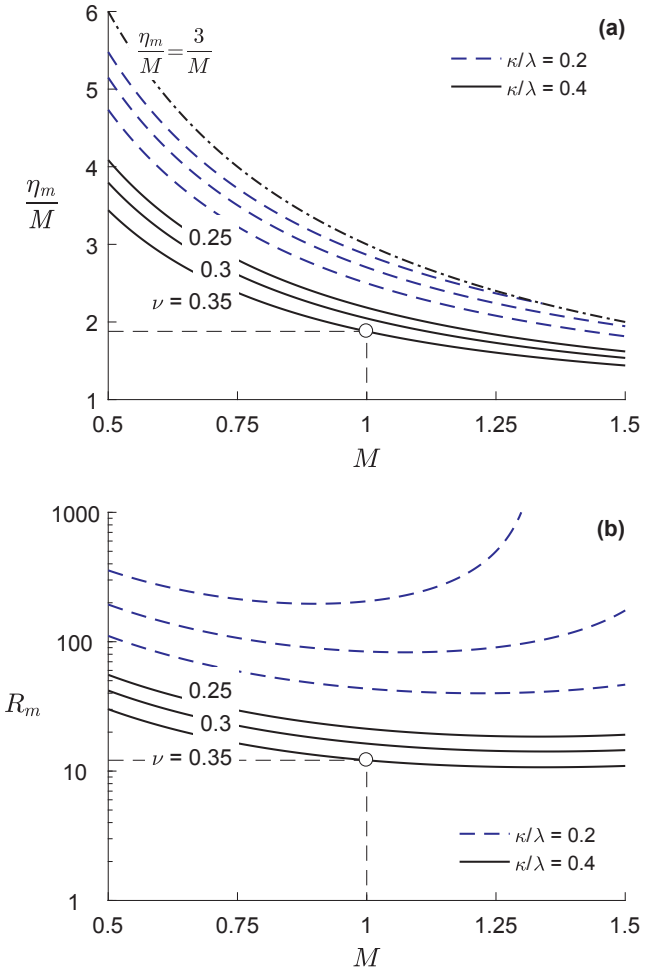

Fig. 10. (a) Normalized snap-back threshold η_m and (b) maximum allowable overconsolidation ratio R_m as a function of the critical stress ratio M for several values of the Poisson's ratio ν and the slope ratio κ/λ, in the case of conventional drained triaxial compression ($\alpha = 3$).

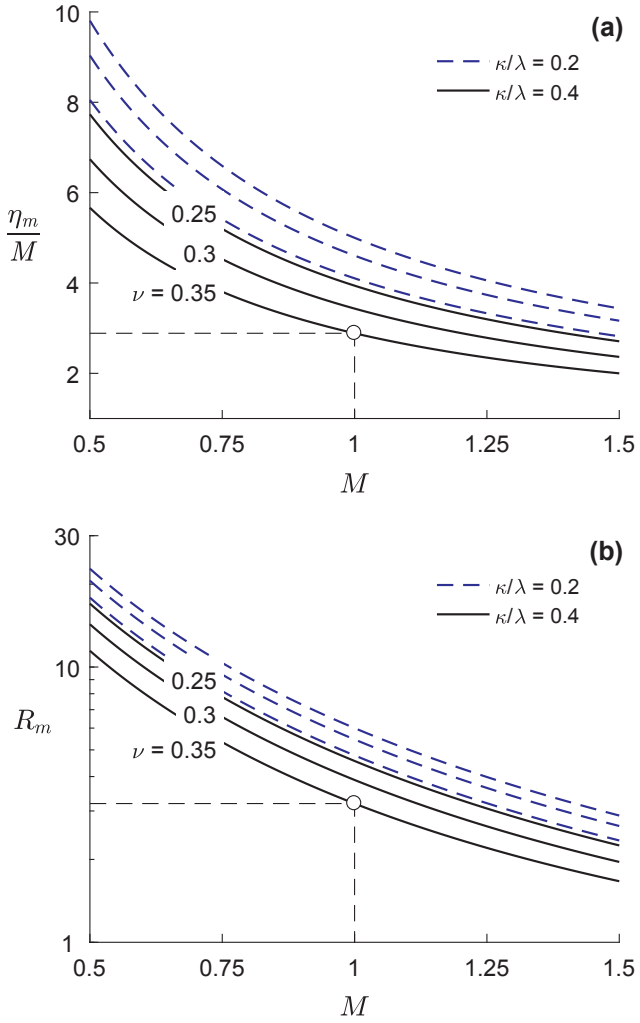

Fig. 11. (a) Normalized snap-back threshold η_m and (b) maximum allowable overconsolidation ratio R_m as a function of the critical stress ratio M for several values of the Poisson's ratio ν and the slope ratio κ/λ, in the case of drained triaxial compression unloading ($\alpha = -3/2$).

the slope ratio κ/λ. Clearly, η_m cannot be higher than the slope α, if $\alpha > 0$ (dash-dot curve in Fig. 10a). Although in the case of conventional triaxial compression the snap-back threshold is associated with high overconsolidation ratios in most of the cases ($R_m = 12.13$ for the set considered here; marked point in Fig. 10b), in the case of triaxial compression unloading, it is associated with very low overconsolidation ratios ($R_m = 3.19$ for the set considered here; marked point in Fig. 11b). This indicates that the computational applicability of the MCC model should be limited to slightly overconsolidated soils in certain cases.

Two examples are analysed in the following in order to illustrate the model behaviour when η_m is exceeded.

4.2.2. Model predictions for conventional triaxial compression

The cases considered for the overconsolidation ratio are the following here: (a) $R = 1.5$ (yielding on the 'wet' side); (b) $R = 10$ (yielding on the 'dry' side; Eq. (46) is satisfied) and; (c) $R = 20$ (yielding on the 'dry' side; Eq. (46) is violated).

For the first two cases (green and blue coloured curves in Fig. 12, respectively), the predicted elasto-plastic response is the expected one: the material hardens and contracts (or softens and dilates), until critical state conditions are reached.

For the third case, where softening exceeds the snap-back threshold, the same behaviour as in Section 4.1 is observed. Specifically, with decreasing deviatoric stress (stress-controlled loading) the response exhibits a snap-back (red solid curves A-A′-B in Fig. 12), while with increasing axial strain (strain-controlled loading) the response deviates from the critical state line (the expansion of the yield surface is unlimited and involves negative plastic strains; red dashed curves A-C in Fig. 12). The reason is again the non-monotonous relationship between the axial strain and the stress ratio η, which presents a turning point at η_m (Fig. 13). It is worth noting again that the plastic multiplier remains always positive in the snap-back case (consider Eqs. (19) and (38)), but uniqueness with respect to the stress ratio η is violated in the range between A and A′.

4.2.3. Model predictions for triaxial compression with constant axial stress

Similar results (with respect to qualitative model behaviour) are also obtained in the case of triaxial compression under constant axial stress and decreasing confining pressure (Figs. 14 and 15), where the following cases were considered: (a) $R = 1$ (yielding on the 'wet' side); (b) $R = 2$ (yielding on the 'dry' side; Eq. (46) is satisfied) and; (c) $R = 4$ (yielding on the 'dry' side; Eq. (46) is violated). As is also depicted in the parametric study in Fig. 11, plastically inadmissible (red dashed curves A-C) and non-unique (red solid curves A-A′) model response is observed for slightly overconsolidated soils here.

4.3. Load case 3: Undrained loading

4.3.1. Governing equations

The final case analysed is the undrained triaxial test. Since deformation occurs under constant volume, the mean effective stress remains constant during elastic response. Therefore, the conditions at yielding are given by Eqs. (32) and (33).

The volumetric part of Eq. (20) becomes

$$\frac{\dot{p}'}{p'} = -\Lambda \frac{2\eta}{M^2 + \eta^2}\dot{\eta}, \tag{47}$$

which after integration gives

$$p'(\eta) = p'_0 \left(\frac{\eta_\rho^2 + M^2}{\eta^2 + M^2} \right)^{\Lambda} \tag{48}$$

(this equation coincides with Eq. (24), since the elasto-plastic stress path lies on the intersection of the SBS in the p'–q–v space with the v_0-plane), while the deviatoric part gives (see also [23] or [37])

$$E_q(\eta) = E_{q\rho} + b(1-2\Lambda)(\eta - \eta_\rho) + \frac{\Lambda}{M} \times \left\{ 2(bM^2-1)\left[\tan^{-1}\left(\frac{\eta}{M}\right) - \tan^{-1}\left(\frac{\eta_\rho}{M}\right) \right] + \ln\left[\frac{(\eta + M)(\eta_\rho - M)}{(\eta - M)(\eta_\rho + M)} \right] \right\}. \tag{49}$$

Eq. (30) together with Eq. (47) implies here that the following inequality should be satisfied on the 'dry' side:

$$f(\eta) = 4\Lambda \frac{\eta^2}{M^4 - \eta^4} + b\left(1 - 2\Lambda \frac{\eta^2}{M^2 + \eta^2}\right) < 0. \tag{50}$$

Under undrained conditions, the plastic multiplier (Eq. (21)) is proportional to the deviatoric strain rate and thus to the function f (after Eq. (29)). Therefore, the function f shares the same solution with the function h in order for the plastic multiplier not to vanish during plastic flow; that is, the snap-back threshold, η_m, coincides with the critical stress ratio for satisfying local uniqueness under pure strain

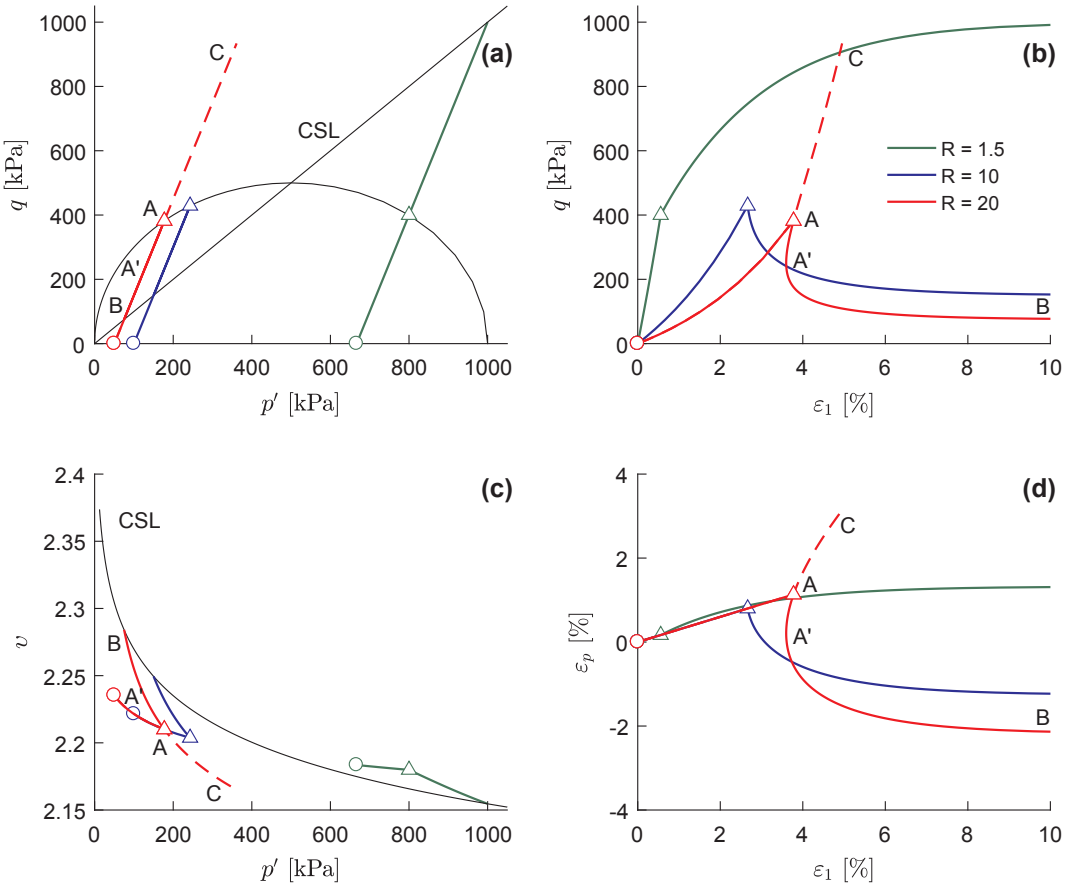

Fig. 12. MCC model predictions for the conventional drained triaxial compression test: (a) mean effective stress vs. deviatoric stress; (b) axial strain vs. deviatoric stress; (c) mean effective stress vs. specific volume and; (d) axial strain vs. volumetric strain.

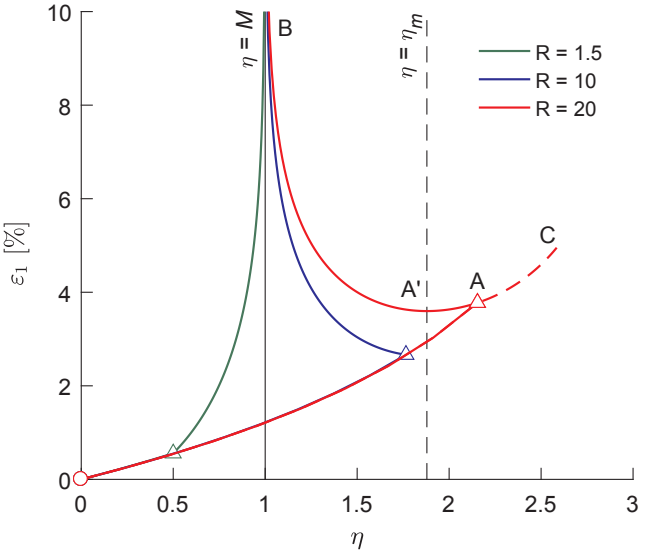

Fig. 13. Axial strain as a function of the stress ratio η for the conventional drained triaxial compression test (example in Fig. 12).

control, η_d. Fig. 7 plots the function f for the parameter set considered. Clearly, the inequality (50) is satisfied, given that this parameter set has been chosen to satisfy the standard condition of local uniqueness. Therefore, the κ/λ ratio is increased to 0.6 here. Fig. 16 plots the corresponding function f as well as function h verifying that $\eta_m = \eta_d = 2.24$.

The maximum allowable overconsolidation ratio can be expressed in closed form here:

$$R \quad < \quad R_m = R_d = 1 + (\eta_d/M)^2, \tag{51}$$

where η_d is given from Eqs. (25) and Eq. (26) (Fig. 4). Fig. 17 shows the maximum allowable overconsolidation ratio R_d under undrained conditions as a function of the critical stress ratio M for several values of the Poisson's ratio and $\kappa/\lambda = 0.5$ and 0.6, complementary to Fig. 4. For the present parameter set, $R_d = 6.00$ (marked point). A specific example is analysed in the following, illustrating the model behaviour when η_d is exceeded.

4.3.2. Model predictions

The following overconsolidation ratios are considered: (a) $R = 1.5$ (yielding on the 'wet' side); (b) $R = 5$ (yielding on the 'dry' side; Eq. (51) is satisfied) and; (c) $R = 6$ (yielding on the 'dry' side; Eq. (51) is violated).

Figs. 18 and 19 plot the predicted response analogously to the previous loading cases. For $R = 1.5$ (green coloured curves) and $R = 5$ (blue coloured curves), the expected elasto-plastic response is observed: the material hardens or softens, respectively. For $R = 7$ (red coloured curves), where $\eta_p > \eta_d$, the predicted response is not admissible for a strain-controlled (red dashed curves) or for a stress-controlled loading process (red solid curves). Specifically, for increasing strain after yielding (point A) the stress ratio η increases (point C), thus leading to a negative plastic multiplier and negative plastic strains. For decreasing stress (or stress ratio) after yielding (point A) the axial strain decreases up to the point A′ (where $\eta = \eta_d$; local uniqueness is violated between A and A′) and then increases moving towards the critical state (point B). Similarly to the previous loading cases, the plastic multiplier remains positive during the snap-back (consider Eqs. (19) and (47)). This is

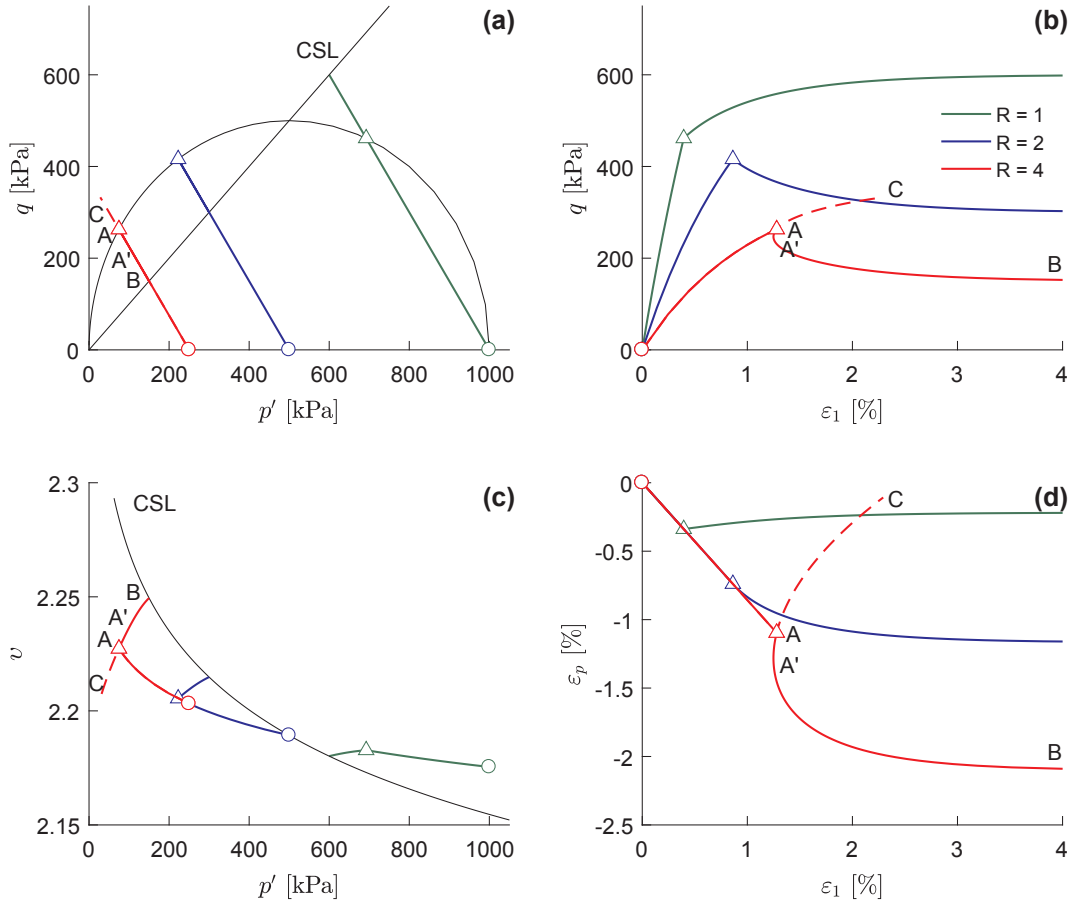

Fig. 14. MCC model predictions for the drained triaxial compression unloading test: (a) mean effective stress vs. deviatoric stress; (b) axial strain vs. deviatoric stress; (c) mean effective stress vs. specific volume and; (d) axial strain vs. volumetric strain.

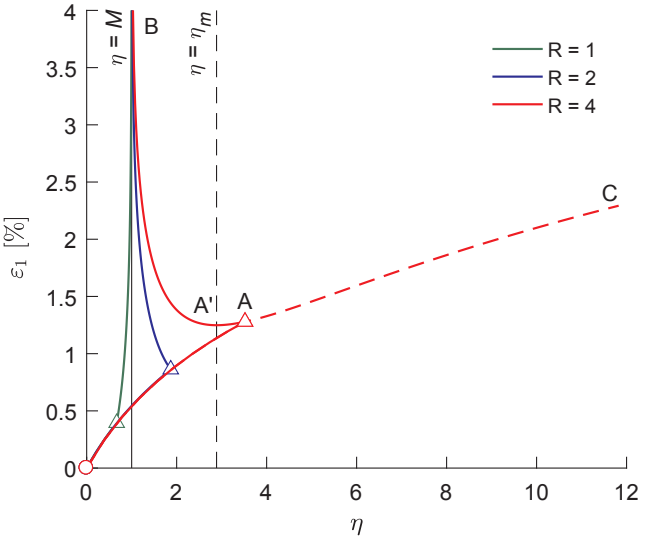

Fig. 15. Axial strain as a function of the stress ratio η for the drained triaxial compression test under constant axial stress (example in Fig. 14).

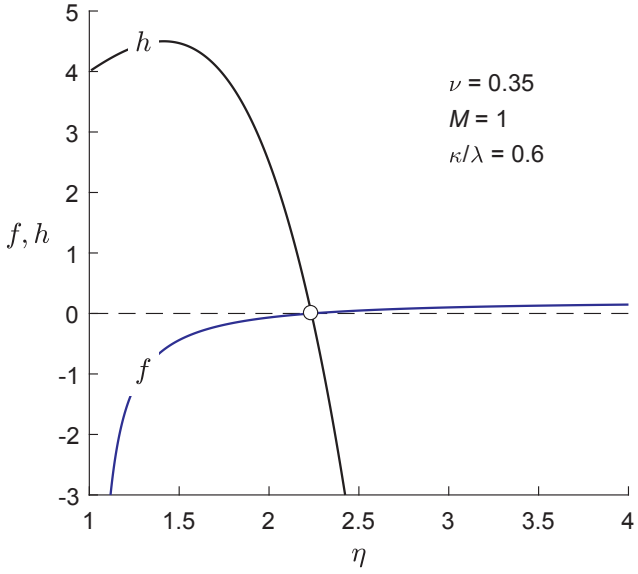

Fig. 16. Representation of the function h (Eq. (22)) and of the function f in undrained loading (Eq. (50)).

explained as follows: for post-yield states between points A and A′ (where axial and deviatoric strains decrease) both the nominator and the denominator of χ (after Eq. (21)) become negative, while for subsequent states between points A′ and B both of them become positive.

5. Implications for the numerical analysis of boundary value problems

It is clear that when $h < 0$ (in pure strain control, *e.g.* undrained loading; Section 3) or $f > 0$ (in mixed stress-strain control, *e.g.*

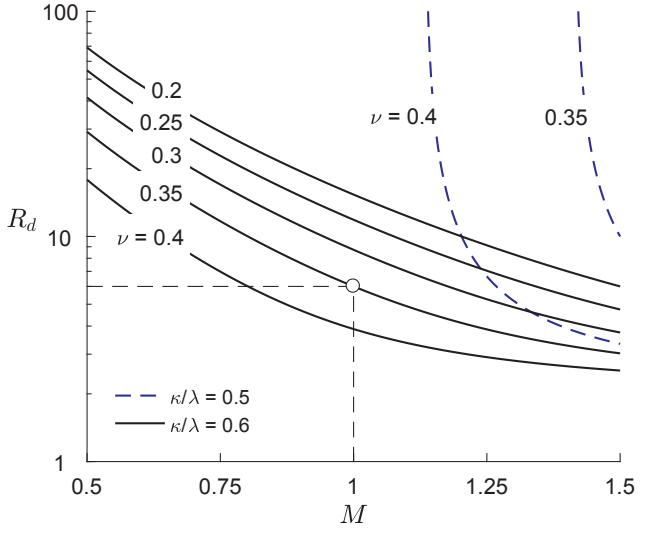

Fig. 17. Maximum allowable overconsolidation ratio R_d as a function of the critical stress ratio M for several values of the Poisson's ratio ν and the slope ratio κ/λ, in the case of undrained loading.

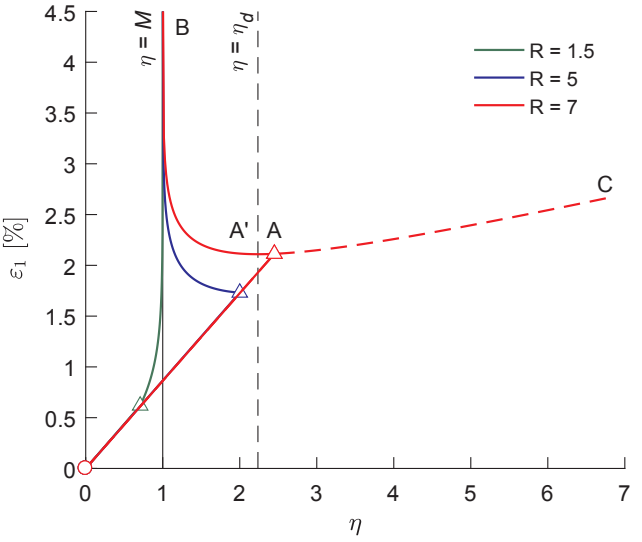

Fig. 19. Axial strain as a function of the stress ratio η for the undrained triaxial compression test (example in Fig. 18).

conventional triaxial compression with constant confinement and increasing axial strain; Section 4) the model response is not unique and the predicted response to a prescribed monotonously increasing strain evolution becomes inadmissible according to plasticity theory. As stress-point algorithms and numerical analysis codes are typically strain- or displacement-based, respectively, it is worth investigating how they behave in simple one-dimensional problems with fixed principal directions, where the above conditions are violated.

The element test results presented in Section 4 can be reproduced by means of a simple explicit integration scheme. Hence, in order to

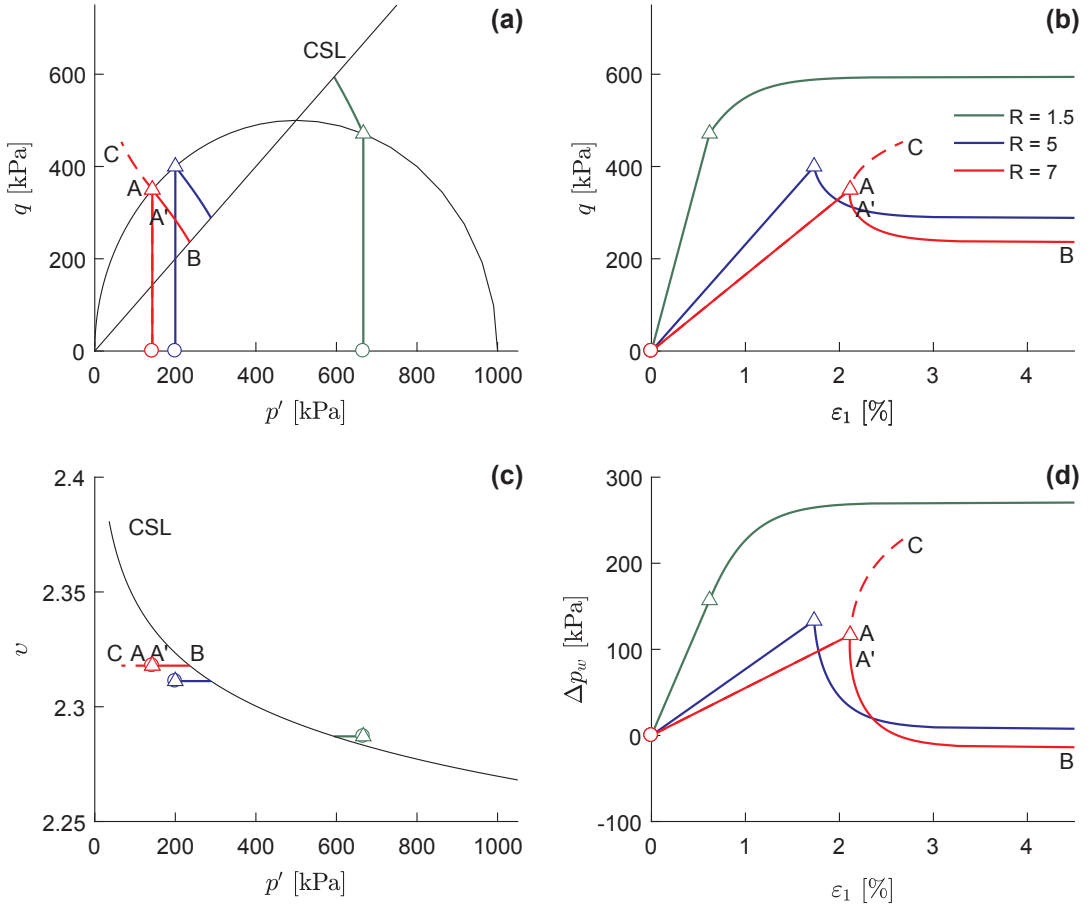

Fig. 18. MCC model predictions for the undrained triaxial compression test: (a) mean effective stress vs. deviatoric stress; (b) axial strain vs. deviatoric stress; (c) mean effective stress vs. specific volume and; (d) axial strain vs. excess pore pressure.

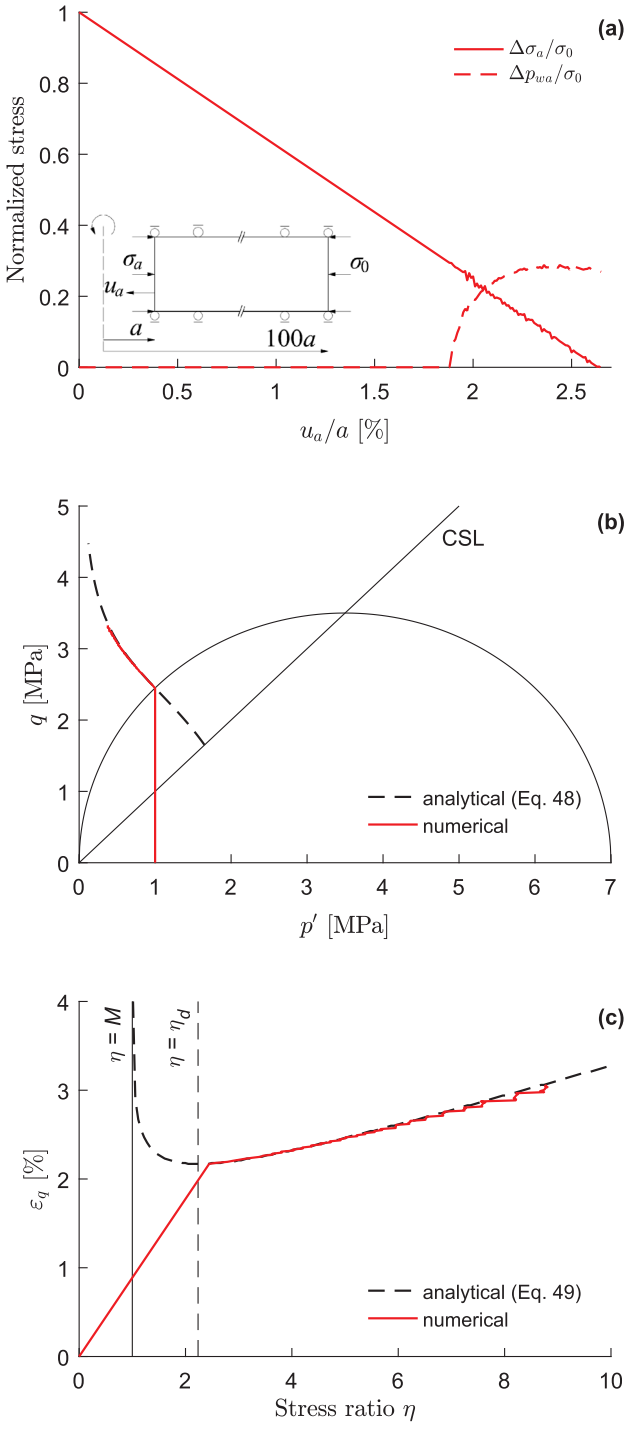

Fig. 20. (a) Normalized total stress and excess pore pressure at the tunnel wall as a function of convergence; (b) effective stress path at the tunnel wall and; (c) deviatoric strain as a function of the stress ratio η at the tunnel wall ($\nu = 0.35$, $\kappa = 0.02$, $\kappa/\lambda = 0.6$, $M = 1$, $\Gamma = 2.5$; $\sigma_0 = 2$ MPa; $p_{w0} = 1$ MPa; $R = 7$).

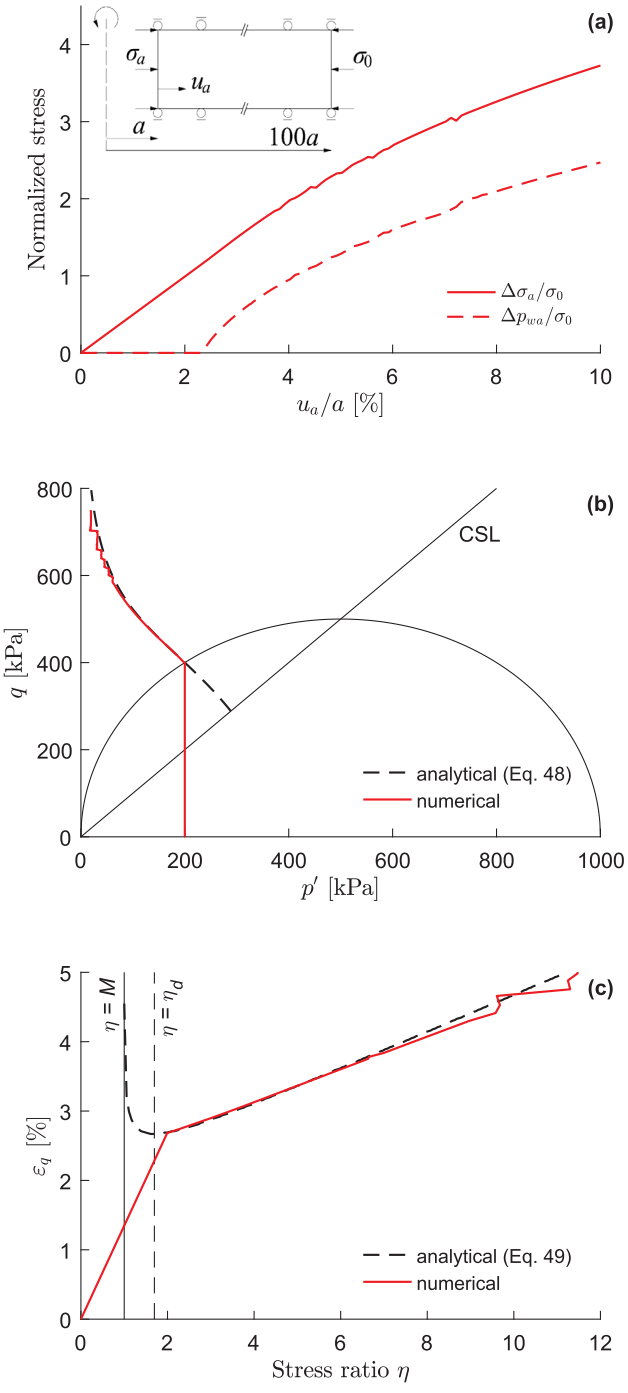

Fig. 21. (a) Normalized total stress and pore pressure at the cavity wall as a function of the cavity expansion; (b) effective stress path at the cavity wall and; (c) deviatoric strain as a function of the stress ratio η at the cavity wall ($\nu = 0.4$, $\kappa = 0.02$, $\kappa/\lambda = 0.6$, $M = 1$, $\Gamma = 2.5$; $\sigma_0 = 200$ kPa; $p_{w0} = 0$; $R = 5$).

demonstrate the model behaviour on a larger scale, the more general examples of undrained cavity contraction (*e.g.* tunnels, boreholes) and expansion (*e.g. in situ* tests, piles) were analysed, given that the stress path in the p'–q plane, the deviatoric strain–stress ratio relationship and the critical stress ratio η_d of any material point around the cavity are still given by Eqs. (48), (49) and (25), respectively. Specifically, in undrained cavity contraction/expansion problems with isotropic initial stress states the deviatoric strain (Eq. (10)) equals $\varepsilon_q = 2\varepsilon_1/\sqrt{3}$, where the major principal strain is the tangential for contraction and the radial for expansion (see among others [37]).

Coupled hydraulic-mechanical computations were performed with the Abaqus finite element code [8], taking a very low permeability value compared to the loading rate. The computational model consists of a horizontal axisymmetric strip of inner radius a and outer radius $100a$. The horizontal boundaries are restrained in the vertical direction,

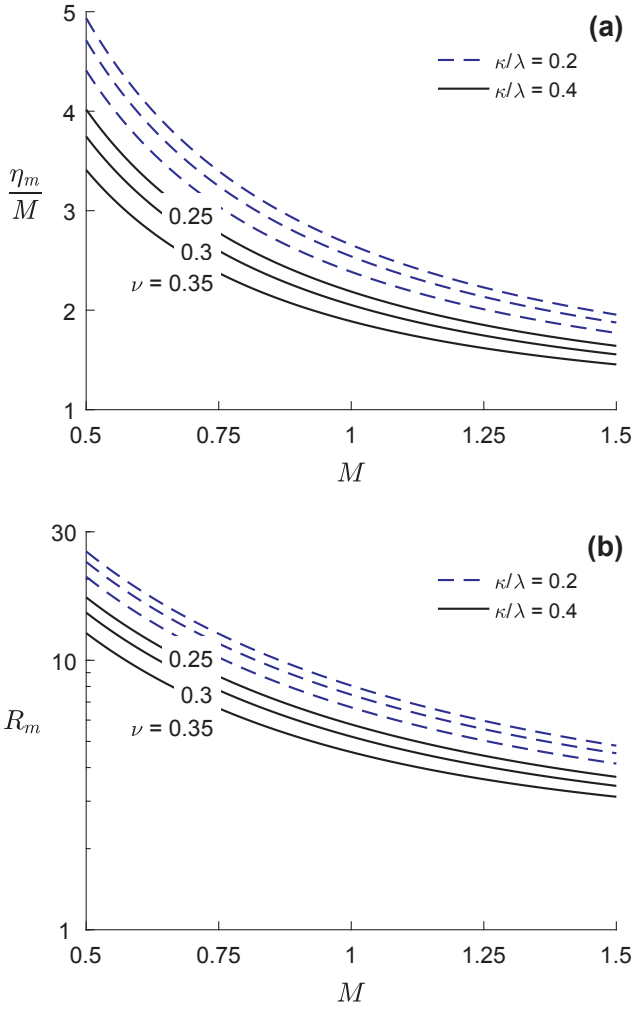

Fig. 22. (a) Normalized snap-back threshold η_m and (b) maximum allowable overconsolidation ratio R_m as a function of the critical stress ratio M for several values of the Poisson's ratio ν and the slope ratio κ/λ, in the case of constant p' loading with $\sigma'_a = \sigma'_3$.

while a stress boundary condition is applied at the far field vertical boundary. The initial stress state is taken as uniform and isotropic. The contraction (or expansion) is modelled by applying an inward (or outward) displacement at the cavity wall.

Fig. 20 shows (a) the predicted total radial stress and excess pore pressure at the cavity wall (determined from the closest integration point) as a function of the cavity convergence, (b) the corresponding effective stress path and (c) the corresponding relationship between the deviatoric strain and the stress ratio η. The response is the same as in Figs. 18 and 19: although yielding occurs on the 'dry' side, the yield surface expands (negative plastic strains thus appear) and the stress path does not move towards the critical state line. As explained earlier (see Fig. 5), the reason for this plastically inadmissible model behaviour is that the stress ratio at yielding (point A) is higher than the uniqueness threshold (turning point A′). Therefore, with increasing strain after yielding, the response follows the path A-C (where η increases) and not the path A-A′-B (where η decreases). Fig. 21 plots similar results for the corresponding cavity expansion problem.

These two examples verify that a finite element analysis code may find a solution that satisfies the basic requirements of equilibrium and compatibility, but will give nonsensical results, since the constitutive behaviour violates plasticity theory. This numerical solution becomes 'unstable' only at very high stress ratios, as indicated by the fluctuations in the stress-strain paths in Figs. 20 and 21.

In more complex boundary value problems, such inadmissible behaviour may occur in part of the model (for example, close to the ground surface where the overconsolidation ratio can increase significantly due to the low *in situ* stresses compared with the preconsolidation pressure), or even in individual integration points. Therefore, it can hardly be detected at all. The most likely scenario, however, is that the algorithm will not be able to converge after (or during) violation of the above conditions in part of the model, and will thus be terminated. The reason is that in more complex problems (unlike one-dimensional ones) it will be practically impossible to find a solution that satisfies equilibrium.

In conclusion, for the avoidance of numerical difficulties, an initial check should be made to verify that the maximum expected stress ratio η, (a), is lower than η_d, which can be evaluated independently of the loading path, and, (b), is lower than η_m, which depends on the loading path (see for example [2] and [18] for characteristic stress paths in common geotechnical problems). Note that in general $\eta_m \leq \eta_d$, while under undrained conditions $\eta_m = \eta_d$. The maximum expected stress ratio η can be estimated from Eq. (32) or Eq. (41), respectively, with reference to the maximum initial overconsolidation ratio of the soil.

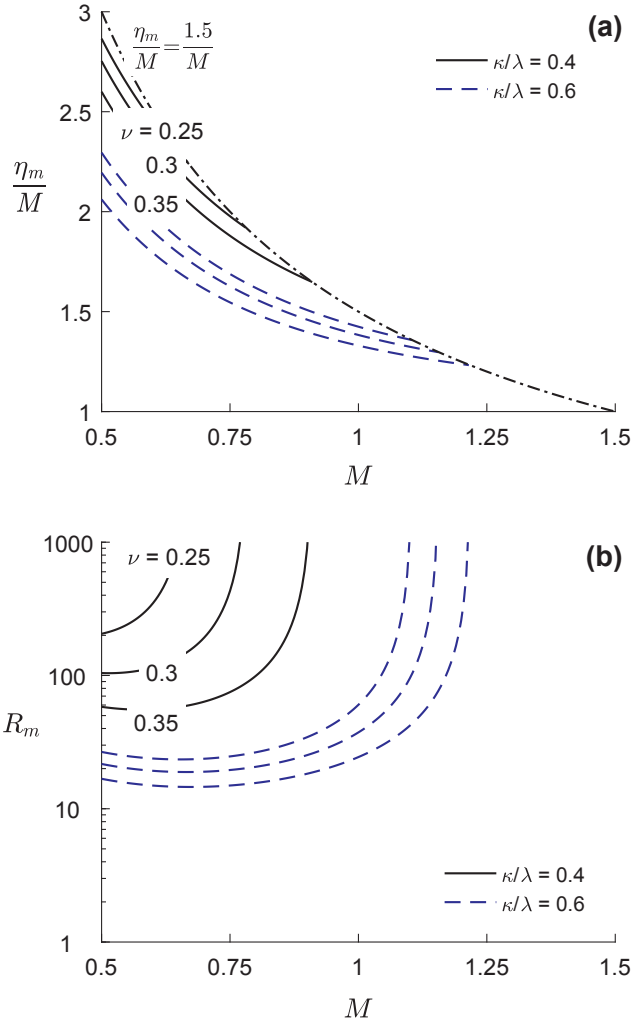

Fig. 23. (a) Normalized snap-back threshold η_m and (b) maximum allowable overconsolidation ratio R_m as a function of the critical stress ratio M for several values of the Poisson's ratio ν and the slope ratio κ/λ, in the case of drained triaxial extension loading ($\alpha = 3/2$).

6. Conclusions

The paper investigated the computational applicability of the MCC model on the 'dry' side. Initially, it was shown that the MCC model satisfies local uniqueness in arbitrary strain-controlled loadings as long as the stress ratio η does not exceed a certain critical value, denoted by η_d and given in closed form, which depends on the Poisson's ratio ν, the κ/λ ratio and the critical stress ratio M. The higher the ν, the κ/λ and the M, the lower the η_d. Theoretical analysis of the basic triaxial compression loadings then showed that the MCC model satisfies local uniqueness in mixed stress- and strain-controlled loadings as long as the stress ratio η does not exceed another critical value, denoted by η_m ($\leq \eta_d$), which depends on the same material constants and on the stress path. If η_m is exceeded (at first yielding), the predicted response in a stress-controlled loading process (*i.e.* for decreasing deviatoric stress or stress ratio) presents a 'snap-back', while in a strain-controlled loading process (*i.e.* for increasing axial strain) it is plastically not allowable as the plastic multiplier becomes negative and the model produces negative plastic strains. Finally, it was shown by means of numerical analysis of two simple boundary value problems with fixed principal axes using a commercial finite element code that displacement-based numerical analysis codes may produce nonsensical results, which violate plasticity theory in cases where the above-threshold values are exceeded.

The results presented may be useful, (a), for evaluating the applicability of the MCC model in computational applications, (b), for finding out the potential reason for numerical difficulties in complex simulations with the MCC model and, (c), for formulating and evaluating refined constitutive models based on the critical state theory.

Acknowledgements

I wish to thank Prof. M. Kavvadas & Dr. A. Kalos (NTU Athens) for the helpful discussion on the topic as well as Prof. G. Anagnostou (ETH Zurich) for his guidance, encouragement and support. I wish also to thank both Reviewers for their constructive comments and suggestions, which were of great help in improving the submitted manuscript.

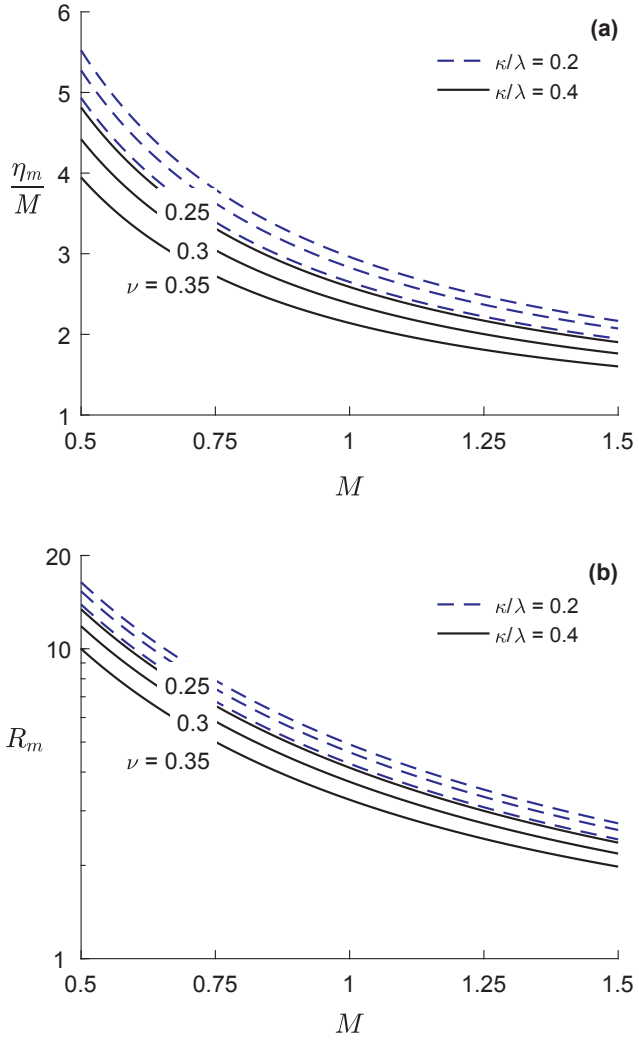

Fig. 24. (a) Normalized snap-back threshold η_m and (b) maximum allowable overconsolidation ratio R_m as a function of the critical stress ratio M for several values of the Poisson's ratio ν and the slope ratio κ/λ, in the case of drained triaxial extension unloading ($\alpha = -3$).

Appendix A. Results for triaxial extension loadings

The entire theoretical analysis of Section 4 refers to triaxial compression, where the axial direction represents the major principal direction. In the case of triaxial extension, where the axial direction represents the minor principal direction, the function f should be modified.

More specifically, the radial (major principal) strain rate is expressed with respect to the strain rate invariants as follows (*cf.* Eq. (29)):

$$\dot{E}_1 = \dot{E}_r = \dot{E}_p/3 + \dot{E}_q/2. \tag{52}$$

Substitution of the volumetric and deviatoric strains from Eq. (20) into Eq. (52) indicates that for any prescribed monotonously increasing strain evolution the following condition should be satisfied (*cf.* Eq. (30)):

$$\dot{E}_1 = \left[\frac{\lambda/\kappa}{3} + \frac{b\eta}{2} + \frac{(\lambda/\kappa-1)\eta}{M^2-\eta^2}\right]\frac{\dot{p}'}{p'} + \left[\frac{b}{2} + \frac{(\lambda/\kappa-1)2\eta}{M^2+\eta^2}\left(\frac{1}{3} + \frac{\eta}{M^2-\eta^2}\right)\right]\dot{\eta} \quad > \quad 0. \tag{53}$$

Then, for constant p' loading (*cf.* Eq. (36)):

$$f(\eta) = \frac{b}{2} + \frac{(\lambda/\kappa-1)2\eta}{M^2+\eta^2}\left(\frac{1}{3} + \frac{\eta}{M^2-\eta^2}\right) \quad < \quad 0, \tag{54}$$

and for drained loading under a linear stress path (*cf.* Eq. (45)):

$$f(\eta) = \left[\frac{\lambda/\kappa}{3} + \frac{b\eta}{2} + \frac{(\lambda/\kappa-1)\eta}{M^2-\eta^2}\right]\frac{1}{\alpha-\eta} + \frac{b}{2} + \frac{(\lambda/\kappa-1)2\eta}{M^2+\eta^2}\left(\frac{1}{3} + \frac{\eta}{M^2-\eta^2}\right) \quad < \quad 0. \tag{55}$$

The function f remains unchanged under undrained loading conditions.

In an analogous manner to Figs. 8, 10 and 11, Figs. 22–24 present (a) the normalized snap-back threshold η_m and (b) the corresponding overconsolidation ratio R_m for the cases of constant p' loading, triaxial extension with increasing radial stress ($\alpha = 3/2$) and triaxial extension with decreasing axial stress ($\alpha = -3$), respectively, considering several values for the significant model parameters.

References

[1] Amorosi A, Kavvadas MJ. A plasticity-based constitutive model for natural soils: a hierarchical approach. In: Kolymnas D, editor. Constitutive modelling of granular materials. Heidelberg: Springer-Verlag; 2000. p. 413–38.
[2] Atkinson JH. Foundations and slopes: an introduction to applications of critical state soil mechanics. London: McGraw-Hill; 1981.
[3] Atkinson JH, Bransby PL. The mechanics of soils: an introduction to the critical state soil mechanics. London: McGraw-Hill; 1978.
[4] Bigoni D, Hueckel T. Uniqueness and localization – I. Associative and non-associative elastoplasticity. Int J Solids Struct 1991;28(2):197–213.
[5] Britto AM, Gunn MJ. Critical state soil mechanics via finite elements. Chichester: Ellis Horwood; 1987.
[6] Borja RI, Lee SR. Cam-clay plasticity, part I: implicit integration of elasto-plastic constitutive relations. Comput Methods Appl Mech Eng 1990;78(1):49–72.
[7] Borja RI. Cam-clay plasticity, part II: implicit integration of constitutive equation based on a nonlinear elastic stress predictor. Comput Methods Appl Mech Eng 1991;88(2):225–40.
[8] Dassault Systèmes. Abaqus 6.12 – theory Manual and analysis user's manual. Dassault Systèmes: Vélizy Villacoublay; 2012.
[9] Federico A, Elia G, Murianni A. The at-rest earth pressure coefficient prediction using simple elasto-plastic constitutive models. Comput Geotech 2009;36(1–2):187–98.
[10] Gens A, Potts DM. Critical state models in computational geomechanics. Eng Comput 1988;5(3):178–97.
[11] Hashash YMA, Whittle AJ. Integration of the modified Cam-Clay model in non-linear finite element analysis. Comput Geotech 1992;14(2):59–83.
[12] Houlsby GT. The use of a variable shear modulus in elastic-plastic models for clays. Comput Geotech 1985;1(1):3–13.
[13] Houlsby GT, Wroth CP, Muir Wood DM. Predictions of the results of laboratory tests on a clay using a critical state model. In: Gudehus G, Darve F, Vardoulakis I, editors. Constitutive relations for soils: results of the international workshop; Grenoble, 6–8 September 1982. Rotterdam: Balkema; 1982. p. 99–121.
[14] Imposimato S, Nova R. An investigation on the uniqueness of the incremental response of elastoplastic models for virgin sands. Mech Cohesive-Frictional Mater 1998;3(1):65–87.
[15] Jirásek M, Bažant ZP. Inelastic analysis of structures. Chisester: Wiley; 2002.
[16] Klisinski M, Mróz Z, Runesson K. Structure of constitutive equations in plasticity for different choices of state and control variables. Int J Plast 1992;8(3):221–43.
[17] Mita KA, Dasari GR, Lo KW. Performance of a three-dimensional Hvorslev–modified Cam clay model for overconsolidated clay. Int J Geomech 2004;4(4):296–309.
[18] Muir Wood D. Soil behaviour and critical state soil mechanics. Cambridge: Cambridge University Press; 1990.
[19] Muir Wood D, Mackenzie NL, Chan AHC. Selection of parameters for numerical predictions. In: Houlsby GT, Schofield AN, editors. Predicted soil mechanics. London: Thomas Telford; 1993. p. 496–512.
[20] Naylor DJ, Pande GN. Finite elements in geotechnical engineering. Swansea: Pineridge Press; 1981.
[21] Nova R. Controllability of the incremental response of soil specimens subjected to arbitrary loading programmes. J Mech Behav Mater 1994;5(2):193–201.
[22] Perić D. Analytical solutions for a three-invariant Cam clay model subjected to drained loading histories. Int J Numer Anal Meth Geomech 2006;30(5):363–87.
[23] Perić D, Ayari MA. On the analytical solutions for the three-invariant Cam clay model. Int J Plast 2002;18(8):1061–82.
[24] Pietruszczak S. Fundamentals of plasticity in geomechanics. Boca Raton: CRC Press; 2010.
[25] Potts DM, Ganendra D. An evaluation of substepping and implicit stress point algorithms. Comput Methods Appl Mech Eng 1994;119(3–4):341–54.
[26] Potts DM, Zdravković L. Finite element analysis in geotechnical engineering: Theory. London: Thomas Telford; 1999.
[27] Potts DM, Zdravković L. Finite element analysis in geotechnical engineering: application. London: Thomas Telford; 2001.
[28] Puzrin AM. Constitutive modelling in geomechanics. Heidelberg: Springer; 2012.
[29] Roscoe KH, Burland JB. On the generalized stress-strain behaviour of 'wet' clay. In: Heyman J, Leckie FA, editors. Engineering plasticity. Camridge: Camridge University Press; 1968. p. 535–609.
[30] Roscoe KH, Schofield AN, Wroth CP. On the yielding of soils. Géotechnique 1958;8(1):22–53.
[31] Schofield AN, Wroth CP. Critical state soil mechanics. London: McGraw-Hill; 1968.
[32] Sheng D, Sloan SW. Load stepping schemes for critical state models. Int J Numer Meth Eng 2001;50(1):67–93.
[33] Sheng D, Sloan SW, Yu HS. Aspects of finite element implementation of critical state models. Comput Mech 2000;26(2):185–96.
[34] Simo JC, Hughes TJR. Computational inelasticity. New York: Springer-Verlag; 1998.
[35] Sloan SW, Abbo AJ, Sheng D. Refined explicit integration of elastoplastic models with automatic error control. Eng Comput 2001;18(1/2):121–54.
[36] Stallebrass SE, Taylor RN. The development and evaluation of a constitutive model for the prediction of ground movements in overconsolidated clay. Géotechnique 1997;47(2):235–53.
[37] Vrakas A, Anagnostou G. Finite strain elastoplastic solutions for the undrained ground response curve in tunnelling. Int J Numer Anal Meth Geomech 2015;39(7):738–61.
[38] Wroth CP. Some aspects of the elastic behaviour of overconsolidated clay. In: R.H.G. Parry, editor. Stress-strain behaviour of soils: proceedings of the Roscoe memorial symposium. Foulis: Henley-on-Thames; 1972. p. 347–61.
[39] Zdravković L, Carter J. Contributions to Géotechnique 1948–2008: constitutive and numerical modelling. Géotechnique 2008;58(5):405–12.
[40] Zienkiewicz OC, Naylor DJ. The adaptation of critical state soil mechanics theory for use in finite elements. In: Parry RHG, editor. Stress-strain behaviour of soils: proceedings of the Roscoe memorial symposium. Foulis: Henley-on-Thames; 1972. p. 537–47.
[41] Zytynski M, Randolph MF, Nova R, Wroth CP. On modelling the unloading-reloading behaviour of soils. Int J Numer Anal Meth Geomech 1978;2(1):87–94.